PCNA-K164 ubiquitination facilitates origin licensing and mitotic DNA synthesis

Wendy Leung[1], Ryan M. Baxley[1,4], Tanay Thakar[2,4], Colette B. Rogers[1], Joseph P. Buytendorp[1], Liangjun Wang[1], Anika Tella[3], George-Lucian Moldovan[2], Naoko Shima[3], and Anja-Katrin Bielinsky[1,5]

[1]Department of Biochemistry, Molecular Biology, and Biophysics, University of Minnesota, Minneapolis, MN 55455, USA

[2]Department of Biochemistry and Molecular Biology, The Pennsylvania State University College of Medicine, Hershey, PA 17033, USA

[3]Department of Genetics, Cell Biology and Development, University of Minnesota, Minneapolis, MN 55455, USA

[4]These authors contributed equally

[5]Lead Contact

[*]Correspondence: bieli003@umn.edu

SUMMARY

Keywords: PCNA; replication stress; origin licensing; mitotic DNA synthesis; FANCD2; genome stability

ABSTRACT

Ubiquitination of the replication clamp proliferating cell nuclear antigen (PCNA) at the conserved residue lysine 164 (K164) occurs during normal S phase progression and increases after DNA damage induced replication stress. This signal is crucial for Okazaki fragment (OF) maturation and for the activation of two DNA damage tolerance pathways; error-prone translesion synthesis and error-free template switching. Recently, we demonstrated that PCNA ubiquitination operates in a fork protection pathway parallel to BRCA-RAD51. However, whether PCNA ubiquitination regulates other genome maintenance mechanisms is unclear. Utilizing *PCNA*^{K164R} cells generated by CRISPR-Cas9 genome editing, we demonstrate that this mutation impacts origin licensing and causes DNA replication defects. Our data suggest that the accumulation of single-stranded (ss) DNA gaps from the previous replication cycle, interferes with the loading of MCM2-7 double hexamers in the following G1 phase. Insufficient origin licensing leads to under-replicated regions throughout the genome that are not resolved by mitotic DNA synthesis (MiDAS). We uncover a novel role for PCNA-K164 ubiquitination in regulating FANCD2 mono-ubiquitination to initiate MiDAS. Our findings demonstrate that the impact of PCNA-K164 ubiquitination is not limited to S/G2 phases but extends to G1 and mitosis.

INTRODUCTION

Maintenance of genome integrity is an intricate process requiring an extended protein network and coordination of many cellular pathways (1). Proper DNA replication is essential to genome maintenance and ensures precise duplication without sections left un-replicated or replicated more than once. Replication can be divided into three phases: origin licensing, origin firing and DNA synthesis (2). Origin licensing occurs during late mitosis and G1 phase, where cell division cycle (CDC) protein 6 (CDC6) and chromatin licensing and DNA replication factor 1 (CDT1) direct the loading of the minichromosome maintenance (MCM) proteins 2-7 (MCM2-7) in a double hexameric complex onto DNA (3–7). As the cell transitions from G1 to S phase, the helicase co-activators CDC45 and the go-ichi-ni-san (GINS) complex are recruited to form the CDC45-MCM2-7-GINS (CMG) helicase (8, 9). To initiate DNA synthesis, a pair of CMG complexes is activated and the recruitment of MCM10, proliferating cell nuclear antigen (PCNA), and DNA polymerases α, ε, and δ occurs to catalyze bidirectional DNA replication (10–13).

A variety of endogenous and exogenous sources of DNA damage can impede replication and generate aberrant fork structures that can lead to chromosomal alterations (14–17). In response to DNA damage or replication fork stalling, PCNA is ubiquitinated at the conserved lysine (K) residue 164, activating DNA damage tolerance (DDT) pathways (18–21). DDT pathways are categorized as either error-prone or error-free. Mono-ubiquitination at K164 by the E2-E3 radiation sensitive (RAD) protein 6 and 18 (RAD6-RAD18) complex activates the error-prone translesion synthesis (TLS) pathway (22, 23). TLS is catalyzed by specialized low-fidelity DNA polymerases to directly bypass DNA lesions (24–26). Mono-ubiquitinated PCNA can be further modified by K63-linked poly-

ubiquitin chains by the E2 ubiquitin conjugating enzyme UBC13-MMS21 and two E3 ligases, helicase-like transcription factor (HLTF) or SNF2 histone linker PHD RING helicase (SHPRH), driving error-free template switching (TS) (27–36). TS utilizes a recombination-like mechanism by which the nascent DNA of the sister chromatid serves as a template for replication (37–42). To facilitate this switch, K63-linked ubiquitin chains recruit the DNA translocase, zinc finger RAN-binding domain containing protein 3 (ZRANB3), to revert the fork (43–47). Given the importance of PCNA-K164 ubiquitination, it is not surprising that mutation of this residue renders cells hypersensitive to DNA damaging agents (48–52). However, how this modification and its associated DDT pathways function in maintaining human genome stability is still not understood.

Regions of the genome that may be particularly reliant on DDT pathways include late-replicating common fragile sites (CFS) (53). Failed replication at specific CFS can be caused by an insufficient number of licensed origins, inefficient origin firing, and failure to activate dormant origins (54–56). Insufficient origin licensing can increase late replication intermediates (LRIs) at CFS as well as other loci, leading to the formation of Fanconi Anemia (FA) group D2 protein (FANCD2) foci during G2/M phase (57, 58). Such LRIs can be resolved through the formation of ultra-fine bridges in anaphase and/or p53-binding protein 1 (53BP1) nuclear bodies (NBs) during the subsequent G1 phase. A recently discovered mechanism to resolve LRIs is mitotic DNA synthesis (MiDAS) (59, 60). MiDAS employs a break-induced replication (BIR)-like process to resolve LRIs and to ensure proper chromosome segregation in anaphase (59–61). While MiDAS in human cancer cells depend on RAD52 (60), we recently demonstrated that this RAD52-driven mechanism is absent in nontransformed human cells. MiDAS in nontransformed human

cells instead relies on FANCD2 (61). Whether PCNA ubiquitination plays any role in MiDAS has not been explored, although both pathways cooperate in DNA crosslink repair (62).

We have recently shown that PCNA-K164 ubiquitination acts in parallel to breast cancer (BRCA) predisposition genes 1 and 2 and the FA pathway to prevent nascent DNA degradation by DNA replication ATP-dependent helicase/nuclease, DNA2 (63). Fork reversal is a mechanism to restart forks, but reversed forks are often subjected to nucleolytic degradation. Loading of RAD51 onto nascent DNA strands at stalled forks by the BRCA1/2-FA pathway prevents MRE11 nuclease-dependent degradation (64–67). When this pathway is defective, PCNA-K164 ubiquitination becomes critical to promote efficient Okazaki fragment (OF) ligation during DNA replication, allowing for proper PCNA unloading and nucleosome deposition, thereby preventing DNA2 nuclease-dependent degradation (63). Thus, both the BRCA1/2-FA and PCNA-K164 ubiquitination pathways function in fork protection. Additionally, Nayak and co-workers revealed that activation of TLS polymerases prevents replication fork slowing and remodeling thereby suppressing ssDNA gap formation and promoting cancer cell fitness. Targeting TLS polymerases with a small-molecule inhibitor not only disrupts DNA replication, but synergizes with gap-inducing therapies, highlighting the importance of replication gaps as a cancer vulnerability (68).

In this study, we demonstrate that PCNA-K164 ubiquitination is critical for accurate DNA replication and genome stability in human cells. Loss of PCNA-K164 ubiquitination in 293T and hTERT RPE-1 (referred to subsequently as RPE-1) cells leads to decreased origin licensing and firing, and impaired DNA synthesis under unperturbed conditions.

These defects generate ssDNA gaps that are not resolved during mitosis. Compromised MiDAS in *PCNA*^{K164R} mutants is directly linked to decreased FANCD2 mono-ubiquitination. Taken together, our data show that PCNA ubiquitination at K164 is not only important for progressive DNA synthesis during S phase, but it promotes efficient origin licensing and facilitates MiDAS to ensure complete genome duplication prior to cell division.

RESULTS

PCNA-K164 ubiquitination is required for DNA damage tolerance in human cells

Previous studies investigating the role of PCNA ubiquitination during DDT in human cells relied on knockdown of endogenous PCNA and overexpression of a K164R mutant or PCNA-ubiquitin fusion constructs (51, 52). To directly test the importance of this post-translational modification, we utilized CRISPR/Cas9 mediated gene targeting to knock-in an A>G mutation in the codon for K164 at the endogenous *PCNA* locus in RPE-1 cells, resulting in expression of a K164R mutant protein (Supplementary Figure S1A). PCR analyses identified mono- and bi-allelic targeting of *PCNA* (Supplementary Figure S1B and C), and subsequent Sanger sequencing confirmed two homozygous $PCNA^{K164R}$ (1E12, 2B10), and one hemizygous $PCNA^{K164R/-}$ (1E4) clones. Karyotype analysis revealed that *PCNA* mutant cell lines 1E12 and 1E4 became tetraploid following the targeting event (Supplementary Figure S1D). All mutants cell lines expressed the same steady-state levels of the licensing factor MCM2 as wildtype (Supplementary Figure S1E). Western blot analyses measuring levels of PCNA ubiquitination after UV irradiation showed a dose-dependent increase in wildtype RPE-1 cells, but not in the $PCNA^{K164R}$ mutant cell lines (Figure 1A). Furthermore, we measured levels of phosphorylated replication protein A (pRPA32) and phosphorylated histone H2AX (γH2AX) as a readout for DNA double-stranded breaks (DSBs). We found a dose-dependent increase in pRPA32 and γH2AX in all cell lines, but the levels were significantly elevated in the K164R mutants (Figure 1A). Due to the increase in DSBs, we investigated the expression of DNA damage induced checkpoint markers phosphorylated p53 (S15), p53, and p21. Low dose UV treatment (10 J/m^2) was sufficient to increase the levels of

all three damage markers in the *PCNA*^{K164R} mutants compared to wildtype (Figure 1B). These observations suggested that ubiquitination of PCNA at K164 confers a response to UV irradiation in human cells.

To further understand the role of PCNA ubiquitination in DNA damage resistance, we utilized 3-(4,5-dimethylthiazol-2-yl)-5-(3-carboxymethoxyphenyl)-2-(4-sulfophenyl)-2H-tetrazolium (MTS) assays to evaluate the sensitivity of *PCNA*^{K164R} mutants to a variety of genotoxic drugs. The mutants were highly sensitive to methyl methanesulfonate (MMS), mitomycin C (MMC) and 4-nitroquinoline 1-oxide (4NQO), but not to hydroxyurea (HU), aphidicolin (APH) or camptothecin (CPT) (Figure 1C). Moreover, cell cycle analysis revealed a G2 arrest in the mutants when challenged with MMS or MMC (Figure 1D and E). Taken together, these data indicate that PCNA-K164 ubiquitination is required for tolerance of lesion-induced replication stress.

PCNA^{K164R} mutants exhibit decreased DNA synthesis caused by reduced origin licensing

RPE-1 *PCNA*^{K164R} mutants exhibited significantly slower cell proliferation compared to wildtype (Figure 2A), contrary to previous studies that reported no significant proliferation defect in yeast, chicken, or mouse cell lines (22, 48, 69, 70). A similar defect was observed in *PCNA*^{K164R} mutant 293T cell lines (Supplementary Figure S2A) (63). Two possibilities could explain the reduced proliferation rate observed in these mutants: (1) slower DNA replication and/or (2) increased cell death. To delineate between these possibilities, we performed flow cytometry analyses of cells stained with propidium iodide (PI) and annexin V. We found a mild but significant increase in early- and late-apoptotic

cells in both tetraploid K164R mutants (1E12 and 1E4) (Figure 2B and C). We also assessed whether DNA replication was slower in the K164R mutants utilizing quantitative chromatin flow cytometry. This allowed us to determine the cell cycle distribution using DAPI-staining for total DNA content in combination with a 30 minute 5-ethynyl-2'-deoxyuridine (EdU) pulse to label S phase cells (Figure 2D, Supplementary Figure S2B). We observed a significant increase in G1 and G2 phase populations and a concomitant decrease in S phase populations in both RPE-1 and 293T *PCNA*^{K164R} cells (Figure 2E, Supplementary Figure S2C). Interestingly, the 293T *PCNA*^{K164R} mutant complemented with wildtype PCNA did not show rescue of the cell cycle defects (Supplementary Figure S2C). This effect could be due to the presence of PCNA trimers composed entirely or partially of K164R mutant PCNA, which would render these trimers non- or hypofunctional, respectively. These data demonstrated that *PCNA*^{K164R} mutants exhibit delayed progression through the G1/S phase transition.

Delayed cell-cycle progression could be attributed to defects in replication origin licensing, DNA synthesis, or a combination of both. To distinguish between these possibilities, we measured chromatin-bound MCM2, as a marker for the MCM2-7 complex to quantify origin licensing in G1 phase, and EdU incorporation into DNA to quantify active DNA synthesis (Figure 3A) (71, 72). *PCNA*^{K164R} mutant cells showed a significant decrease in EdU incorporation (Figure 2F, Supplementary Figure S2D), consistent with previous reports suggesting that K164 ubiquitination has a role during normal DNA replication (63, 69, 73, 74). Surprisingly, we observed an MCM2 loading defect in the RPE-1 *PCNA*^{K164R} mutants, as a significant decrease in the mean fluorescent intensity (MFI) of G1 loaded MCM2 was detected (Figure 3B and D). Furthermore, the percentage

of cells with MCM2 efficiently loaded onto chromatin specifically in late G1 was significantly reduced in the mutants compared to wildtype (Figure 3C and E). A similar defect was observed in the 293T *PCNA*^{K164R} mutant (Supplementary Figure S3). Altogether, these data suggest a previously unknown connection between PCNA-K164 ubiquitination and origin licensing.

PCNA^{K164R} mutants display DNA replication defects and accumulate under-replicated DNA

To understand the DNA synthesis defects in *PCNA*^{K164R} cells, we performed DNA combing analysis under unperturbed conditions. Due to the origin licensing defect observed in these mutants, we predicted longer inter-origin distances (IODs). Whereas wildtype cells displayed a median IOD of ~93 kb, the median IOD in *PCNA*^{K164R} RPE-1 mutants, 1E12 and 1E4, markedly increased to ~115 kb (Figure 4A and B). This difference equates to ~19% fewer origins fired in these tetraploid mutants. Although the median IOD in *PCNA*^{K164R} mutant 2B10 increased to ~106 kb, which equates to ~12% fewer origins fired, this increase was not statistically significant compared to wildtype. These data are consistent with the fact that the diploid mutant (2B10) had a 20% reduction in origin licensing, which is significantly less than the 50% reduction in the tetraploid mutants (1E12 and 1E4). In line with the observed increase in IODs, we observed a 30-50% decrease in new origin firing events in all *PCNA*^{K164R} mutants regardless of cell type (Figure 4A and C, Supplementary Figure S4A). Next, we measured global fork speed and stability. Average fork speed was modestly increased in the *PCNA*^{K164R} cells (Figure 4D) (63), consistent with previous studies showing that suppression of origin firing results in

faster fork progression (75–78). Fork stability, however, was not changed (Figure 4E). These findings indicate that the K164R mutation compromises the number of active replication forks due to diminished origin licensing.

As fewer origins were licensed and activated, we hypothesized that some regions of the genome would remain under-replicated (57, 79–81). One fate of under-replicated DNA persisting into mitosis is the conversion into large chromatin domains known as 53BP1 NBs, which are sequestered and inherited by daughter cells (82–85). To investigate whether *PCNA*^{K164R} mutants have an elevated number of under-replicated regions, we analyzed 53BP1 NB formation in G1 nuclei. *PCNA*^{K164R} mutants had a 3-fold increase in 53BP1 NBs compared to wildtype under unperturbed conditions (Figure 4F, Supplementary Figure S4B). Low-level replication stress induced by APH treatment (300 nM) led to a 3-to-5-fold increase in 53BP1 NB formation in the wildtype cells, however, there was no additional increase in NBs in the mutant cells. Given that *PCNA*^{K164R} mutants have a similar sensitivity to APH as the wildtype cells (Figure 1C), the lack of an increase in 53BP1 NB formation suggested that mutant cells: (1) experience maximal replication stress under steady-state conditions, (2) resolve LRIs via alternative mechanism(s), or (3) undergo chromosome mis-segregation. Interestingly, the 293T *PCNA*^{K164R} mutant complemented with wildtype PCNA partially rescued the APH sensitivity (Supplementary Figure S4B). Taken together, our data clearly demonstrate that ubiquitination of PCNA at K164 is required for complete genome duplication to prevent the inheritance of under-replicated regions by daughter cells following cell division.

PCNA-K164 ubiquitination regulates MiDAS through the mono-ubiquitination of FANCD2

Defects in origin licensing increase FANCD2 foci at certain loci during G2/M phases of the cell cycle, which activates MiDAS as the cells final attempt to complete DNA replication prior to cell division (61). To visualize MiDAS, we pulse-labeled cells with EdU and examined its incorporation and co-localization with FANCD2 in prophase/prometaphase nuclei (53). Knockdown of MCM4, an essential component of the replicative helicase, decreases origin licensing genome-wide (81, 86, 87) and led to increased EdU and FANCD2 foci (Supplementary Figure S5A-C), consistent with previous data that showed elevated EdU and FANCD2 foci following origin recognition complex subunit 1 (ORC1) depletion (61). Given the observed defect in origin licensing in *PCNA*^{K164R} cells, we suspected that these mutants would upregulate MiDAS to minimize under-replicated DNA passing through mitosis. Surprisingly, RPE-1 *PCNA*^{K164R} cells had significantly fewer FANCD2 foci (~4-fold) despite an increase in LRIs, which subsequently led to a decrease in MiDAS (~6-fold) compared to wildtype cells (Figure 5A-C, Supplementary Figure S6A). Similar results were seen in the 293T *PCNA*^{K164R} mutant. Interestingly, the 293T *PCNA*^{K164R} mutant complemented with wildtype PCNA partially restored FANCD2 foci formation, however it was not sufficient to rescue the MiDAS phenotype (Figure 5D and E, Supplementary Figure S6B). These findings suggest a role for PCNA-K164 ubiquitination in regulating MiDAS through the recruitment and/or mono-ubiquitination of FANCD2.

We previously have shown that depletion of FANCA, a component of the FA core complex involved in the mono-ubiquitination of FANCD2, significantly impaired MiDAS

(61). Furthermore, since mono-ubiquitinated FANCD2 binds tightly to DNA (88, 89) and is a prerequisite for focus formation, we focused our attention on understanding whether K164 ubiquitination mediates FANCD2 mono-ubiquitination. We found that under unperturbed conditions, FANCD2 mono-ubiquitination was drastically reduced in the RPE-1 *PCNA*^{K164R} cells. Interestingly, upon inducing low-level replication stress by exposure to APH (300 nM), FANCD2 mono-ubiquitination was elevated in the RPE-1 and 293T wildtype cells, but not in the *PCNA*^{K164R} mutants (Figure 5F and G). The decrease in FANCD2 mono-ubiquitination observed in the mutants was not due to an overall reduction in steady-state levels of cellular FANCD2 (Figure 5F, WCE).

Since RAD18-mediated PCNA-K164 ubiquitination has been previously linked to FANCD2 mono-ubiquitination (90, 91), we generated *RAD18*$^{-/-}$ single and *RAD18*$^{-/-}$*:PCNA*^{K164R} double mutants and examined them for mitotic EdU incorporation and FANCD2 foci formation. *RAD18*$^{-/-}$ cells displayed approximately 50% fewer EdU and FANCD2 foci compared to wildtype. However, *RAD18*$^{-/-:}$*PCNA*^{K164R} double mutants had similar levels of EdU and FANCD2 foci as *PCNA*^{K164R} single mutants, consistent with RAD18 acting upstream of PCNA ubiquitination (Figure 5A-C, Supplementary Figure S6A). These results are in agreement with reports that two other E3 ubiquitin ligases, ring finger protein 8 (RNF8) and Cullin-4-RING-ligase (CRL4)-Ddb1-Cdt2 (CRL4^{Cdt2}) are capable of mono-ubiquitinating PCNA (92, 93). These results suggest that in the absence of RAD18, PCNA ubiquitination by alterative E3 ligases partially activates MiDAS. In contrast, when PCNA is unable to be ubiquitinated at K164, MiDAS is severely compromised. Taken together, these data indicate that PCNA-K164 plays a critical role

in activating MiDAS in response to under-replicated DNA through the mono-ubiquitination of FANCD2.

DISCUSSION

Here, we uncover novel roles for ubiquitination of PCNA-K164 in maintaining genome stability by resolving LRIs through MiDAS and promoting efficient origin licensing in the subsequent G1 by suppressing ssDNA gaps (Figure 6). In addition, we recently provided evidence that in the absence of PCNA ubiquitination during unperturbed conditions, ssDNA gaps accumulated during lagging strand synthesis, which lead to defects in OF maturation (63). We propose that these lagging strand gaps cause the significant reduction in DNA synthesis observed in *PCNA*^{K164R} mutant cells (Figure 2F, Supplementary Figure S2D). In this study, we corroborate that under-replicated DNA persists into the next cell cycle (Figure 4E, 5B-E, Supplementary Figure S4B) due to reduced FANCD2 mono-ubiquitination and severely compromised activation of MiDAS (Figure 5B-G). Furthermore, the continuous increase in ssDNA gaps from previous rounds of DNA replication causes insufficient origin licensing in G1 (Figure 3, Supplementary Figure S3), thereby exacerbating the under-replication phenotype.

PCNA-K164 ubiquitination is essential to maintain genome stability

The inability to ubiquitinate PCNA at K164 severely inhibited faithful genome duplication. Consistent with previous studies in mammalian cells, our *PCNA*^{K164R} mutants were sensitive to DNA damage induced by UV, MMS, and MMC (Figure 1) (47, 50–52). Contrary to studies of *PCNA*^{K164R} mouse embryonic fibroblasts (47), we did not detect any additional sensitivity to CPT-induced replication stress compared to wildtype, consistent with an earlier report in human cells (51). This discrepancy could be due to differences in mouse and human cells, as viable *PCNA*^{K164R} mice were generated (70),

whereas this mutation has never been identified in human tissues. However, these mice were sterile and exhibited bone marrow (BM) failure, as well as defects in somatic hypermutation and class switch recombination (70, 94, 95), implying that K164 ubiquitination is not completely dispensable in mice. Interestingly, the infertility and BM phenotype in the *PCNA*^{K164R} mice are shared phenotypes with FA mouse models (96, 97).

The sensitivity of *PCNA*^{K164R} mutant cells primarily to lesion-induced DNA damage (Figure 1) (63) suggests that these cells rely on TLS in response to certain types of replication stress. Over a decade ago, multiple groups demonstrated that TLS occurs on both the leading and lagging strands in response to DNA damage induced replication stress (98–101). Lagging strand blocks do not impact leading strand synthesis, as lagging strand synthesis can be restarted by re-priming. However, due to inefficient leading strand re-priming, these blocks can stall DNA synthesis and cause fork uncoupling while DNA unwinding and lagging strand synthesis continues at a reduced rate (102, 103). These observations suggested that lesions encountered on the leading strand impact replication fork progression more significantly than lagging strand lesions. Interestingly, a recent paper demonstrated that TLS occurs mainly “on the fly” on the leading strand to restart uncoupled replication forks, whereas TLS on the lagging strand occurs by post-replicative gap filling (104). Our experiments in human cells extend these observations and suggest that K164 ubiquitination is a conserved mechanism by which PCNA regulates TLS on both strands.

The primary function of TLS is to suppress ssDNA gap formation (68). In the absence of TLS polymerase η, there is a significant increase in MiDAS (105, 106).

Elevated levels of MiDAS could be a compensatory mechanism to counteract an increase in ssDNA gaps. Ubiquitination of PCNA at K164 functions to recruit polymerase η for TLS and regulate MiDAS. Thus, without K164 ubiquitination, ssDNA gaps persist which may contribute to the origin licensing defects observed in *PCNA*^{K164R} mutants.

There is a growing body of evidence that suggests that PCNA-K164 ubiquitination is not only induced by DNA damage, but occurs during normal DNA replication (63, 69, 73, 74). We show that both RPE-1 and 293T *PCNA*^{K164R} mutants have a significant reduction in proliferation rate (Figure 2A, Supplementary Figure S2A), and a subtle, but significant global DNA synthesis defect (Figure 2F, Supplementary Figure S2D). The primary replication defects in *PCNA*^{K164R} cells were reduced origin licensing and dormant origin firing (Figure 3E and 4C, Supplementary Figure S3D and S4A). In agreement with these observations, we show that *PCNA*^{K164R} cells have increased IODs (Figure 4B). Given that the rate of origin firing and fork speed are inversely regulated (75–78), we find that fork speed in *PCNA*^{K164R} cells was also modestly increased (Figure 4D) (63). Interestingly, the increase in fork speed observed in the *PCNA*^{K164R} cells is similar to changes observed in cells depleted of ligase I (LIG1) or flap endonuclease I (FEN1), factors involved in lagging strand synthesis (107). Recently, we have shown that PCNA ubiquitination plays a critical role in OF maturation in budding yeast. Loss of *CDC9* (LIG1), *RAD27* (FEN1), and the PCNA unloader *ELG1* (ATAD5), trigger PCNA ubiquitination (108, 109). Moreover, we performed a synthetic genetic array (SGA) screen by crossing a PCNA-K164R mutant to a deletion mutant array containing every viable knock-out open reading frame of the yeast genome and examined the similarity of their genetic interaction signatures. We found that the signature of the K164R mutant mimicked those of strains

defective in lagging strand synthesis including *RFC5*, *POL31* (Pol δ), *RAD27*, and *ELG1* mutants (110). Likewise, we show that human *PCNA*^{K164R} cells phenocopy the DNA synthesis defects seen in LIG1 and FEN1 depleted cells, further supporting a conserved role for PCNA ubiquitination in promoting OF processing (63) by gap suppression.

Absence of PCNA ubiquitination leads to the accumulation of ssDNA gaps that interfere with OF ligation. Previous studies of licensing in budding yeast utilizing electron microscopy, single-molecule and *in vitro* reconstitution experiments revealed that MCM2-7 hexamers were loaded cooperatively in a head-to-head orientation onto double-stranded (ds) DNA (5, 6, 111). Furthermore, activation of CMG to initiate DNA synthesis relies on a mechanism in which the complex tracks with force, and with the recruitment of MCM10, it causes the dsDNA to melt and allow paired CMG complexes to bypass one another on ssDNA (13). Thus, replication initiation only occurs during the transition from dsDNA to ssDNA. Furthermore, poly(ADP-ribose) polymerase (PARP) acts as a sensor of unligated OF fragments (112). We found that defects in OF processing in *PCNA*^{K164R} cells leads to the accumulation of chromatin-bound PAR chains (63). With the MCM2 loading defect (Figure 4C, Supplementary Figure S3C and D) and increased under-replication (Figure 4F, Supplementary Figure S4B) observed in the *PCNA*^{K164R} cells, we propose that accumulation of ssDNA gaps and PAR chains on the lagging strand during the previous S phase prevents efficient loading of MCM2-7 double hexamers in the subsequent G1 phase. Future studies utilizing genome-wide ligation of 3'-OH ends followed by sequencing (GLOE-Seq) would allow for mapping and quantification of these lagging strand gaps in *PCNA*^{K164R} mutant cells to identify whether specific genomic loci are affected (113).

53BP1 NBs in G1 delay replication of under-replicated loci until late S phase by recruiting replication timing regulatory factor 1 (RIF1) (114). This process protects under-replicated DNA from aberrant processing and genotoxic RAD51-mediated recombination. During late S phase, RAD52-mediated repair of under-replicated DNA allows for complete duplication of the locus. Thus, an alternative model to ssDNA gap accumulation preventing origin licensing is that in the absence of PCNA-K164 ubiquitination, persistent under-replicated DNA that is not resolved by MiDAS is converted into 53BP1 NBs, which can directly inhibit origin licensing.

MiDAS activation by FANCD2 is dependent on PCNA ubiquitination

Our observation that *PCNA*^{K164R} cells have a defect in MiDAS reveals an unexpected role for K164 ubiquitination in regulating this process (Figure 5B-E, Supplementary Figure S6A and B). A similar defect was observed in *RAD18*$^{-/-}$ cells (Figure 5B and C), and *RAD18*$^{-/-}$*:PCNA*^{K164R} double mutant cells had no additional MiDAS defect compared to the *PCNA*^{K164R} single mutant, confirming that both are in the same pathway. These data suggest that RAD18-dependent K164 ubiquitination accounts for only ~50% of the MiDAS defect observed in *PCNA*^{K164R} cells, implying that other E3 ligases are utilized to activate MiDAS. Future studies will be needed to address whether RNF8, CRL4^{Cdt2} or another E3 ubiquitin ligase ubiquitinates PCNA to partially activate MiDAS in the absence of RAD18.

FANCD2 has been identified as a key regulator of MiDAS in noncancerous cells (61), but the mechanism of its recruitment to chromatin remained unclear. PCNA and FANCD2 co-localize following HU- and APH-induced replication stress (115, 116). Thus,

FANCD2 could be recruited to chromatin by either unmodified PCNA, through its PCNA-interacting peptide (PIP) box (117), and/or by ubiquitinated PCNA through its coupling of ubiquitin conjugation to endoplasmic reticulum degradation (CUE) domain (118). Recent studies have demonstrated that unmodified FANCD2 does not bind to DNA (88, 89). FANCD2 exists as a homodimer but in response to replication stress, FANCI is exchanged for one subunit of FANCD2, forming a FANCD2-FANCI (D2-I) heterodimer that adopts an open conformation capable of binding DNA. Binding of DNA converts the D2-I complex into a closed conformation, and ubiquitination of FANCD2 by the FA core complex locks the complex on the DNA (88, 89). Moreover, it is known that mono-ubiquitination of FANCD2 is carried out by the E3 ligase FANCL (119, 120). RAD18-mediated PCNA-K164 ubiquitination is required for the recruitment of FANCL to chromatin, which in turn stimulates FANCD2 mono-ubiquitination (90). We demonstrate that *PCNA*^{K164R} cells have reduced levels of mono-ubiquitinated FANCD2 on chromatin when challenged with APH, although FANCD2 levels in WCEs were unaltered (Figure 5F and G). Based on these observations, we speculate that FANCD2 is initially recruited to under-replicated regions by PCNA. However, FANCD2 retention depends on its mono-ubiquitination through K164 ubiquitination-mediated recruitment of FANCL, and this step is defective in the *PCNA*^{K164R} mutants.

It has been suggested that the FA pathway plays a role in DNA synthesis and cell cycle progression, distinct from its role in the repair of replication-associated DNA damage. Specifically, the recruitment of CDC45 to initiate replication is dependent on FANCD2 mono-ubiquitination (121). We observed defects in both dormant origin firing (Figure 4C, Supplementary Figure S4A) and MiDAS (Figure 5A-E) in *PCNA*^{K164R} cells,

processes that are also dependent on the mono-ubiquitination of FANCD2. Future studies will be required to understand if PCNA-K164 ubiquitination promotes replication initiation through FANCD2 mono-ubiquitination.

MATERIALS AND METHODS

Cell lines

RPE-1 cells were grown in Dulbecco's Modified Eagle Medium: Nutrient Mixture F12 (DMEM/F12, Gibco 11320) supplemented with 10% fetal bovine serum (FBS, Sigma F4135) and 1% Penicillin-Streptomycin (Pen Strep, Gibco 15140). 293T cells were grown in Dulbecco's Modified Eagle Medium (DMEM, Gibco 11995) supplemented with 10% FBS and 1% Pen Strep. Cells were cultured at 37 ˚C and 5% CO_2.

Generation of *PCNA^{K164R}*, *RAD18$^{-/-}$*, *RAD18$^{-/-}$:PCNA^{K164R}* cell lines using CRISPR-Cas9

A guide RNA (gRNA) targeting PCNA exon 5 was designed (gRNA: 5'-ATACGTGCAAATTCACCAGA -3') and cloned into a CRISPR/Cas9 (clustered regularly interspaced short palindromic repeats/CRISPR associated 9) plasmid (hSpCas9(BB)-2A-GFP/PX458; Addgene plasmid #48138) as described previously (122). To generate a *PCNA^{K164R}* mutant cell line, a double stranded donor plasmid containing the desired K164R mutation was constructed using Golden Gate cloning and designed as described previously (123–126). Silent mutations were introduced into the donor plasmid to generate a novel restriction enzyme recognition site. RPE-1 wildtype cells were transfected with the CRISPR/Cas9 plasmid containing the PCNA gRNA and the donor plasmid containing the K164R mutation using the Neon Transfection System (Invitrogen MPK5000) following standard protocols. Two days post-transfection GFP-expressing cells were collected by flow cytometry and subcloned. Subclones were screen for correct targeting by PCR amplification and restriction enzyme digestion (Forward: 5'-

TGGCGCTAGTATTTGAAGCA -3', Reverse: 5'- ACTTGGGATCCAATTCTGTCTACT -3', Restriction Enzyme: EcoRI, NEB R3101). Specific mutations were identified by Sanger sequencing (Sequencing: 5'- AGGTGTTGCCTTTTAAGAAAGTGAGG -3').

To generate *RAD18*$^{-/-}$ and *RAD18*$^{-/-}$*:PCNA*^{K164R} mutant cell lines, a guide RNA targeting RAD18 exon 2 (gRNA: 5'- AGACAATAGATGATTTGCTG -3') was designed such that DNA cleavage would disrupt an endogenous restriction enzyme recognition site and was subsequently cloned into a CRISPR/Cas9 plasmid as described above. RPE-1 wildtype cells and *PCNA*^{K164R} 2B10 cells were transfected with the CRISPR/Cas9 plasmid containing the RAD18 gRNA using the Neon Transfection System following standard protocols. Two days post-transfection GFP-expressing cells were collected by flow cytometry and subcloned. Subclones were screen for correct targeting by PCR amplification and restriction enzyme digestion (Forward: 5'- GTAGTACCATGCCGAAAGCAC -3', Reverse: 5'- GGAACCACCTATCTGTTATCC -3', Restriction Enzyme: TseI, NEB R0591). Knockout lines were identified by Sanger sequencing (Sequencing: 5'- CTACCTCATGTAAAAATCGC -3') and Tracking of Indels by DEcomposition (TIDE) analyses (127). 293T *PCNA*^{K164R} lines were generated as described previously (63).

Cell Proliferation

Cells were plated at 100,000 cells per well (RPE-1) or 125,000 cells per well (293T) in 6-well plates. Cell counts were performed 3-days after seeding using Trypan Blue

(Invitrogen T10282) on Countess slides (Invitrogen C10283) using a Countess automated cell counter (Invitrogen C20181).

MTS Cell Viability Assay

RPE-1 cells were plated at 500 cells (wildtype) or 1000 cells (*PCNA*^{K164R}) per well in 96-well plates and allowed to recover for 24 h. Stock solutions of each drug were prepared in sterile 1X phosphate-buffered saline (PBS), water or dimethyl sulfoxide (DMSO) as appropriate and further diluted in growth medium. Cells were allowed to grow for 96 h (methyl methanesulfonate, Acros Organics 156890250, mitomycin C, Sigma M4287, 4-nitroquinoline 1-oxide, Sigma N8141, hydroxyurea, Acros Organics 151680250; aphidicolin, Sigma A0781; camptothecin, Sigma C9911) in drug containing medium and cell viability was measured with the CellTiter 96 Aqueous One Solution Cell Proliferation Assay (Promega G3580) following manufacturer's instructions. The viability of drug treated cells was normalized to the average viability of the untreated control cells for each cell line. Plates were imaged using a VICTOR^{3}V 1420 Multilabel Counter (Perkin Elmer). Analysis and statistical test were performed using Microsoft Excel.

Protein Extraction, Chromatin Fractionation and Western Blotting

For preparation of whole cell extracts, cells were lysed in NETN (20 mM Tris-HCl, pH 8.0, 100 mM NaCl, 1 mM EDTA, 0.5% NP-40 and protease inhibitors) buffer for 10 minutes at 4 ˚C and then centrifuged at 12,000 rpm for 10 minutes at 4 ˚C. Cleared lysates were collected and protein concentrations were determined using Bradford protein assay (Bio-Rad 5000006). Lysates were then mixed with SDS loading buffer and denatured at 95 ˚C

before fractionation by SDS-PAGE and analyses by western blot. Chromatin fractions were isolated as previously described (27, 128). Briefly, extracts were prepared by lysis in Buffer A (10 mM HEPES pH 7.9, 10 mM KCl, 1.5 mM $MgCl_2$, 0.34 M sucrose, 10% glycerol, 0.1% triton X-100 and protease inhibitors) for 5 minutes at 4 ˚C. Insoluble nuclear proteins were isolated by centrifugation at 1300 g at 4 ˚C and chromatin bound proteins were subsequently released by sonication after being resuspended in TSE buffer (20 mM Tris-HCl, pH 8.0, 500 mM NaCl, 2 mM EDTA, 0.1% SDS, 0.1% triton X-100 and protease inhibitors). Remaining insoluble factors were cleared by centrifugation at 17000 g at 4 ˚C. Protein concentrations of chromatin fractions were determined using Bradford protein assay prior to fractionation by SDS-PAGE and western blot analyses. Primary antibodies were incubated in 5% BLOT-QuickBlocker (G-Biosciences 786-011) as follows: mouse anti-PCNA (Abcam, ab29; 1:3000), rabbit anti-Ubiquityl-PCNA (Lys164) (Cell Signaling, D5C7P, 13439; 1:1000), rabbit anti-RPA32 (S4/8) (Bethyl, A300-245A; 1:2000), rabbit anti-γH2AX (Bethyl, A300-081A; 1:2000), rabbit anti-H2AX (Bethyl, A300-082A; 1:5000), rabbit anti-p-p53 (S15) (Cell Signaling, 9284S; 1:500), mouse anti-p53 (Santa Cruz, sc-126; 1:2000), rabbit anti-p21 (Santa Cruz, sc-397 clone C19; 1:1000), rabbit anti-FANCD2 (Abcam, ab108928; 1:2000), rabbit anti-RAD18 (Bethyl, A300-340A; 1:1000), rabbit anti-MCM2 (Cell Signaling, 4007S; 1:1000; BD Biosciences, 610701; 1:1000), rabbit anti-MCM3 (Cell Signaling, 4012S; 1:1000), rabbit anti-MCM4 (Cell Signaling, 3228S; 1:1000); rabbit anti-MCM7 (Cell Signaling, 3757S; 1:1000), mouse anti-GAPDH (GeneTex, GTX627408; 1:10000), mouse anti-Ku86 (Santa Cruz, B-1, sc-5280; 1:500), mouse anti-α-tubulin (Millipore, T9026, clone DM1A; 1:10000). Secondary antibodies were incubated in 5% BLOT-QuickBlocker as follows: goat anti-mouse HRP conjugate (BioRad, 1706516;

1:5000), donkey anti-rabbit HRP conjugate (Amersham, NA9340; 1:5000). Detection was performed using WesternBright Quantum detection kit (K-12042-D20). Quantification was performed using FIJI and Microsoft Excel. Image preparation was performed using Adobe Photoshop.

FACS Analysis

For flow cytometry analyses of cell cycle, RPE-1 wildtype and *PCNA*^{K164R} cells were seeded at 250,000 cells per 10 cm plate and allowed to recover for 24 h. Cells were then treated with methyl methanesulfonate (10 μM) or mitomycin C (20 nM) for 48 h. After, cells were fixed using cold 70% ethanol, washed twice with 1X PBS, and stained with propidum iodide (PI) staining buffer (0.1% triton X-100, 0.2 mg/mL RNase, 40 μg/mL PI, 1 mM EDTA) for 30 minutes at room temperature (RT). Flow samples were processed on a LSR II (BD Biosciences) flow cytometer and analyzed with FlowJo v10.4.2. and Microsoft Excel.

For flow cytometry analyses of cell cycle distribution, DNA synthesis and origin licensing, wildtype and *PCNA*^{K164R} RPE-1 and 293T cells were treated as described previously (Matson, eLife, 2017). Briefly, cells were incubated with 10 μM EdU (Lumiprobe, 20540) for 30 minutes before harvesting with trypsin. Cells were then washed with cold 1X PBS and lysed in CSK (10 mM PIPES pH 7.0, 300 mM sucrose, 100 mM NaCl, 3 mM $MgCl_2$ hexahydrate) with 0.1% triton X-100, then fixed in PBS with 4% paraformaldehyde (Electron Microscopy Services) for 15 minutes. Cells were labeled with AF647-azide (Life Technologies, A10277) in 100 mM ascorbic acid, 1 mM $CuSO_4$, and PBS to detect EdU

for 30 minutes at RT. Cells were then washed and incubated with anti-MCM2 antibody (BD Biosciences, #610700; 1:200) in 1% bovine albumin serum (BSA) in PBS with 0.5% NP-40 for 1 h at 37 °C. Next, cells were washed and labeled with donkey anti-mouse AF488 secondary antibody (Invitrogen, A11029; 1:1000) in 1% BSA in PBS with 0.5% NP-40 for 1 h at 37 °C. Lastly, cells were washed and incubated in DAPI (Life Technologies, D1306; 1 µg/mL) and RNAse A (Sigma, R6513; 100 ng/mL) for 1 h at 37 °C. Samples were processed on a LSR II (BD Biosciences) flow cytometer and analyzed with FlowJo v10.6.1 and Microscoft Excel.

For flow cytometry analyses of apoptosis, RPE-1 wildtype and *PCNA*^{K164R} cells were seeded in 6-well plates at 75,000 cells per well and allowed to proliferate for approximately 72 h. Cells were collected, washed twice with 1X PBS and stained using the APC Annexin V apoptosis detection kit (Biolegend 640932) according to the manufacturer's instructions. Samples were processed on a LSRII (BD Biosciences) flow cytometer. Apoptotic cells were identified by annexin V staining while cell viability was determined by PI staining. Data was analyzed using FlowJo v10.6.1 and Microsoft Excel.

DNA combing

For genome-wide analyses of DNA replication, wildtype and *PCNA*^{K164R} RPE-1 and 293T cells were plated at 40% confluency in 10 cm plates 24 h prior to labeling. Cells were incubated with 25 or 100 µM IdU (Sigma C6891) for 30 minutes, rinsed twice with pre-warmed medium and then incubated with 100 µM or 200 µM CldU (Sigma I7125) for 30 minutes. Approximately 250,000 cells were embedded in 0.5% agarose plugs (NuSieve

GTG Agarose, Lonza, 50080) and digested for 48 h in plug digestion solution (10 mM Tris-HCl, pH 7.5, 1% Sarkosyl, 50 mM EDTA and 2 mg/mL Proteinase K). Plugs were then melted in 50 mM MES pH 5.7 (Calbiochem #475893) and digested overnight with β-agarase (NEB M0392). DNA was then subsequently combed onto commercially available vinyl silane-coated coverslips (Genomic Vision COV-001). Integrity of combed DNA for all samples was quality checked via staining with YOYO-1 (Invitrogen Y3601). Combed coverslips were baked at 60 °C for 2-4 h, cooled to RT and stored at -20 °C. DNA was denatured in 0.5 M NaOH and 1 M NaCl for 8 minutes at RT. All antibody staining was performed in 2% BSA in PBS-Triton (0.1%). Primary antibodies included rabbit anti-ssDNA (IBL 18731), mouse anti-BrdU/IdU (BD Biosciences 347580; clone B44) and rat anti-BrdU/CldU (Abcam, ab6326; BU1/75 (ICR1)). Secondary antibodies included goat anti-mouse Cy3.5 (Abcam ab6946), goat anti-rat Cy5 (Abcam ab6565) and goat anti-rabbit BV480 (BD Horizon #564879). Imaging was performed using Genomic Vision EasyScan service. Images were blinded and analyzed using the Genomic Vision FiberStudio software. Data/statistical analyses were performed in Microsoft Excel and GraphPad Prism 8.

Small-interfering RNA (siRNA) transfection

RPE-1 cells were seeded on coverslips (Thermo Fisher 3405) in 6-well plates and allowed to recover for 24 h. Cells were treated with MCM4 siRNA using Lipofectamine RNAiMAX (Thermo Fisher 13778) in Opti-MEM (Thermo Fisher 31985062) supplemented with 3% FBS for 48 h.

Immunostaining

For immunofluorescent staining of 53BP1 nuclear bodies and Cyclin A, wildtype and *PCNA*^{K164R} RPE-1 and 293T cells were seeded onto fibronectin (Sigma F4759) coated coverslips at 100,000 cells per coverslip and allowed to recover for 24 h. Cells were then treated with 300 nM aphidicolin (Sigma A0781) for 24 h. After, cells were washed with PBS containing 0.9 mM $CaCl_2$ and 0.49 mM $MgCl_2$ (PBS-Ca^{2+}/Mg^{2+}) and fixed in PBS-Ca^{2+}/Mg^{2+} with 4% formaldehyde (Fisher Scientific F79-500) for 10 minutes at RT. Next, cells were washed twice with PBS-Ca^{2+}/Mg^{2+}, permeabilized with 0.1% triton X-100 for 5 minutes at RT, and subsequently blocked in ABDIL (20 mM Tris-HCl, pH 7.5, 150 mM NaCl, 2% BSA, 0.2% Fish Gelatin, 0.1% NaN_3) for 1 h at RT. Coverslips were incubated with rabbit anti-53BP1 (Abcam, ab36823; 1:500) and mouse anti-Cyclin-A (Santa Cruz; sc-271682 clone B8; 1:200) primary antibodies overnight at 4 °C. Next day, coverslips were washed with PBS-Ca^{2+}/Mg^{2+} containing 0.1% Tween 20 and incubated with Alexa Fluor 488 donkey anti-rabbit (Invitrogen, A21206; 1:1000) and Alexa Fluor 594 goat anti-mouse (Invitrogen, A11032; 1:000) secondary antibodies for 1 h at RT. Lastly, coverslips were washed, stained with DAPI (Life Technologies, D1306; 1 µg/mL), and mounted on microscope slides with Vectorshield anti-fade reagent (Vector Laboratories H1000). 30-50 fields per coverslip were imaged on the Zeiss Spinning Disc confocal (University of Minnesota Imaging Center). Images were scored using FIJI and statistical analyses were performed in GraphPad Prism 8.

For immunofluorescent staining of FANCD2 and EdU foci, RPE-1 and 293T lines were seeded onto fibronectin coated coverslips and treated with 300 or 450 nM APH when

applicable. Cells were then washed with PBS and incubated with 20 μM EdU for 30 minutes before fixation with 10% formalin. Fixed cells on coverslips were then subjected to a Click-Chemistry Reaction (20 μM Biotin-Azide, 10 mM sodium ascorbate, and 2 mM $CuSO_4$ in PBS) at RT for 1 h. After, coverslips were washed with PBS and incubated with rabbit anti-FANCD2 (Abcam, ab108928; 1:250) and mouse anti-phospho-Histone H3 (S10) (Cell Signaling; 9706S; 1:200) primary antibodies in PBS containing 0.3% triton X-100 and 1% BSA at 4 °C overnight. The next day, coverslips were washed with PBS and incubated with Alexa Fluor 488 Streptavidin (Thermo Fisher S32354; 1:100), Alexa Fluor 350 anti-mouse (Thermo Fisher A11045; 1:100) and Alexa Fluor anti-rabbit (Thermo Fisher A31632; 1:1000) secondary antibodies at RT for 1 h. Lastly, coverslips were washed with PBS and mounted on microscope slides with Prolong Gold anti-fade reagent (Thermo Fisher P36931). EdU and FANCD2 foci were scored using a Zeiss Axio Imager A1 fluorescent microscope. 300-400 cells per cell line were scored per experiment. Statistical analyses were performed in GraphPad Prism 8.

REFERENCES

1. Barnes,R. and Eckert,K. (2017) Maintenance of genome integrity: How mammalian cells orchestrate genome duplication by coordinating replicative and specialized DNA polymerases. *Genes (Basel).*, **8**.
2. Fragkos,M., Ganier,O., Coulombe,P. and Méchali,M. (2015) DNA replication origin activation in space and time. *Nat. Rev. Mol. Cell Biol.*, **16**, 360–374.
3. Donovan,S., Harwood,J., Drury,L.S. and Diffley,J.F.X. (1997) Cdc6p-dependent loading of Mcm proteins onto pre-replicative chromatin in budding yeast. *Proc. Natl. Acad. Sci. U. S. A.*, **94**, 5611–5616.
4. Seki,T. and Diffley,J.F.X. (2000) Stepwise assembly of initiation proteins at budding yeast replication origins in vitro. *Proc. Natl. Acad. Sci. U. S. A.*, **97**, 14115–14120.
5. Remus,D., Beuron,F., Tolun,G., Griffith,J.D., Morris,E.P. and Diffley,J.F.X. (2009) Concerted Loading of Mcm2-7 Double Hexamers around DNA during DNA Replication Origin Licensing. *Cell*, **139**, 719–730.
6. Evrin,C., Clarke,P., Zech,J., Lurz,R., Sun,J., Uhle,S., Li,H., Stillman,B. and Speck,C. (2009) A double-hexameric MCM2-7 complex is loaded onto origin DNA during licensing of eukaryotic DNA replication. *Proc. Natl. Acad. Sci. U. S. A.*, **106**, 20240–20245.
7. Siddiqui,K., On,K.F. and Diffley,J.F.X. (2013) Regulating DNA Replication in Eukarya. *Cold Spring Harb. Perspect. Biol.*, **5**, 1–17.
8. Bochman,M.L. and Schwacha,A. (2008) The Mcm2-7 Complex Has In Vitro Helicase Activity. *Mol. Cell*, **31**, 287–293.
9. Moyer,S.E., Lewis,P.W. and Botchan,M.R. (2006) Isolation of the Cdc45/Mcm2-7/GINS (CMG) complex, a candidate for the eukaryotic DNA replication fork helicase. *Proc. Natl. Acad. Sci. U. S. A.*, **103**, 10236–10241.
10. Rivera-Mulia,J.C. and Gilbert,D.M. (2016) Replication timing and transcriptional control: Beyond cause and effect - part III. *Curr. Opin. Cell Biol.*, **40**, 168–178.
11. Burgers,P.M.J. and Kunkel,T.A. Eukaryotic DNA Replication Fork.
12. Baxley,R.M. and Bielinsky,A.K. (2017) Mcm10: A dynamic scaffold at eukaryotic replication forks. *Genes (Basel).*, **8**, 13–16.
13. Langston,L.D. and O'Donnell,M.E. (2019) An explanation for origin unwinding in eukaryotes. *Elife*, **8**, 1–17.
14. Macheret,M. and Halazonetis,T.D. (2015) DNA Replication Stress as a Hallmark of Cancer. *Annu. Rev. Pathol. Mech. Dis.*, **10**, 425–448.
15. Técher,H., Koundrioukoff,S., Nicolas,A. and Debatisse,M. (2017) The impact of replication stress on replication dynamics and DNA damage in vertebrate cells. *Nat. Rev. Genet.*, **18**, 535–550.
16. Tubbs,A. and Nussenzweig,A. (2017) Endogenous DNA Damage as a Source of Genomic Instability in Cancer. *Cell*, **168**, 644–656.
17. Primo,L.M.F. and Teixeira,L.K. (2020) Dna replication stress: Oncogenes in the spotlight. *Genet. Mol. Biol.*, **43**, 1–14.
18. Friedberg,E.C. (2005) Suffering in silence: The tolerance of DNA damage. *Nat. Rev. Mol. Cell Biol.*, **6**, 943–953.

19. Chang,D.J. and Cimprich,K.A. (2009) DNA damage tolerance: When it's OK to make mistakes. *Nat. Chem. Biol.*, **5**, 82–90.
20. Ghosal,G. and Chen,J. (2013) DNA Damage Tolerance : A Double Edged Sword Guarding the Genome. *Transl. Cancer Res.*, **2**, 107–129.
21. Leung,W., Baxley,R.M., Moldovan,G.L. and Bielinsky,A.K. (2019) Mechanisms of DNA damage tolerance: post-translational regulation of PCNA. *Genes (Basel).*, **10**.
22. Hoege,C., Pfander,B., Moldovan,G.L., Pyrowolakis,G. and Jentsch,S. (2002) RAD6-dependent DNA repair is linked to modification of PCNA by ubiquitin and SUMO. *Nature*, **419**, 135–141.
23. Davies,A.A., Huttner,D., Daigaku,Y., Chen,S. and Ulrich,H.D. (2008) Activation of Ubiquitin-Dependent DNA Damage Bypass Is Mediated by Replication Protein A. *Mol. Cell*, **29**, 625–636.
24. Shcherbakova,P. V. and Fijalkowska,I.J. (2006) Translesion synthesis DNA polymerases and control of genome stability. *Front. Biosci.*, **11**, 2496–2517.
25. Lehmann,A.R., Niimi,A., Ogi,T., Brown,S., Sabbioneda,S., Wing,J.F., Kannouche,P.L. and Green,C.M. (2007) Translesion synthesis: Y-family polymerases and the polymerase switch. *DNA Repair (Amst).*, **6**, 891–899.
26. Sale,J.E., Lehmann,A.R. and Woodgate,R. (2012) Y-family DNA polymerases and their role in tolerance of cellular DNA damage. *Nat. Rev. Mol. Cell Biol.*, **13**, 141–152.
27. Motegi,A., Liaw,H.-J., Lee,K.-Y., Roest,H.P., Maas,A., Wu,X., Moinova,H., Markowitz,S.D., Ding,H., Hoeijmakers,J.H.J., *et al.* (2008) Polyubiquitination of proliferating cell nuclear antigen by HLTF and SHPRH prevents genomic instability from stalled replication forks. *Proc. Natl. Acad. Sci.*, **105**, 12411–12416.
28. Broomfield,S., Chow,B.L. and Xiao,W. (1998) MMS2, encoding a ubiquitin-conjugating-enzyme-like protein, is a member of the yeast error-free postreplication repair pathway. *Proc. Natl. Acad. Sci. U. S. A.*, **95**, 5678–83.
29. Hofmann,R.M. and Pickart,C.M. (1999) Enzyme Functions in Assembly of Novel Polyubiquitin Chains for DNA Repair. **96**, 645–653.
30. Ulrich,H.D. (2000) Two RING finger proteins mediate cooperation between ubiquitin-conjugating enzymes in DNA repair. *EMBO J.*, **19**, 3388–3397.
31. Brusky,J., Zhu,Y. and Xiao,W. (2000) UBC13, a DNA-damage-inducible gene, is a member of the error-free postreplication repair pathway in Saccharomyces cerevisiae. *Curr. Genet.*, **37**, 168–174.
32. Stelter,P. and Ulrich,H.D. (2003) Control of spontaneous and damage-induced mutagenesis by SUMO and ubiquitin conjugation. *Nature*, **425**, 188–191.
33. Branzei,D., Seki,M. and Enomoto,T. (2004) Rad18/Rad5/Mms2-mediated polyubiquitination of PCNA is implicated in replication completion during replication stress. *Genes to Cells*, **9**, 1031–1042.
34. Unk,I., Hajdu,I., Fatyol,K., Szakal,B., Blastyak,A., Bermudez,V., Hurwitz,J., Prakash,L., Prakash,S. and Haracska,L. (2006) Human SHPRH is a ubiquitin ligase for Mms2-Ubc13-dependent polyubiquitylation of proliferating cell nuclear antigen. *Proc. Natl. Acad. Sci. U. S. A.*, **103**, 18107–18112.
35. Unk,I., Hajdu,I., Fatyol,K., Hurwitz,J., Yoon,J.-H., Prakash,L., Prakash,S. and Haracska,L. (2008) Human HLTF functions as a ubiquitin ligase for proliferating cell nuclear antigen polyubiquitination. *Proc. Natl. Acad. Sci.*, **105**, 3768–3773.

36. Motegi,A., Sood,R., Moinova,H., Markowitz,S.D., Liu,P.P. and Myung,K. (2006) Human SHPRH suppresses genomic instability through proliferating cell nuclear antigen polyubiquitination. *J. Cell Biol.*, **175**, 703–708.
37. Vanoli,F., Fumasoni,M., Szakal,B., Maloisel,L. and Branzei,D. (2010) Replication and recombination factors contributing to recombination-dependent bypass of DNA lesions by template switch. *PLoS Genet.*, **6**.
38. Minca,E.C. and Kowalski,D. (2010) Multiple Rad5 Activities Mediate Sister Chromatid Recombination to Bypass DNA Damage at Stalled Replication Forks. *Mol. Cell*, **38**, 649–661.
39. Branzei,D. (2011) Ubiquitin family modifications and template switching. *FEBS Lett.*, **585**, 2810–2817.
40. Gonzalez-Huici,V., Szakal,B., Urulangodi,M., Psakhye,I., Castellucci,F., Menolfi,D., Rajakumara,E., Fumasoni,M., Bermejo,R., Jentsch,S., *et al.* (2014) DNA bending facilitates the error-free DNA damage tolerance pathway and upholds genome integrity. *EMBO J.*, **33**, 327–340.
41. Fumasoni,M., Zwicky,K., Vanoli,F., Lopes,M. and Branzei,D. (2015) Error-Free DNA Damage Tolerance and Sister Chromatid Proximity during DNA Replication Rely on the Polα/Primase/Ctf4 Complex. *Mol. Cell*, **57**, 812–823.
42. Branzei,D. and Szakal,B. (2016) Priming for tolerance and cohesion at replication forks. *Nucleus*, **7**, 8–12.
43. Ciccia,A., Nimonkar,A. V., Hu,Y., Hajdu,I., Achar,Y.J., Izhar,L., Petit,S.A., Adamson,B., Yoon,J.C., Kowalczykowski,S.C., *et al.* (2012) Polyubiquitinated PCNA Recruits the ZRANB3 Translocase to Maintain Genomic Integrity after Replication Stress. *Mol. Cell*, **47**, 396–409.
44. Weston,R., Peeters,H. and Ahel,D. (2012) ZRANB3 is a structure-specific ATP-dependent endonuclease involved in replication stress response. *Genes Dev.*, **26**, 1558–1572.
45. Yuan,J., Ghosal,G. and Chen,J. (2012) The HARP-like Domain-Containing Protein AH2/ZRANB3 Binds to PCNA and Participates in Cellular Response to Replication Stress. *Mol. Cell*, **47**, 410–421.
46. Badu-Nkansah,A., Mason,A.C., Eichman,B.F. and Cortez,D. (2016) Identification of a substrate recognition domain in the replication stress response protein zinc finger ran-binding domain-containing protein 3 (ZRANB3). *J. Biol. Chem.*, **291**, 8251–8257.
47. Vujanovic,M., Krietsch,J., Raso,M.C., Terraneo,N., Zellweger,R., Schmid,J.A., Taglialatela,A., Huang,J.W., Holland,C.L., Zwicky,K., *et al.* (2017) Replication Fork Slowing and Reversal upon DNA Damage Require PCNA Polyubiquitination and ZRANB3 DNA Translocase Activity. *Mol. Cell*, **67**, 882-890.e5.
48. Arakawa,H., Moldovan,G.L., Saribasak,H., Saribasak,N.N., Jentsch,S. and Buerstedde,J.M. (2006) A role for PCNA ubiquitination in immunoglobulin hypermutation. *PLoS Biol.*, **4**, 1947–1956.
49. Edmunds,C.E., Simpson,L.J. and Sale,J.E. (2008) PCNA Ubiquitination and REV1 Define Temporally Distinct Mechanisms for Controlling Translesion Synthesis in the Avian Cell Line DT40. *Mol. Cell*, **30**, 519–529.
50. Hendel,A., Krijger,P.H.L., Diamant,N., Goren,Z., Langerak,P., Kim,J., Reißner,T., Lee,K. young, Geacintov,N.E., Carell,T., *et al.* (2011) PCNA ubiquitination is

important, but not essential for translesion DNA synthesis in mammalian cells. *PLoS Genet.*, **7**.
51. Niimi,A., Brown,S., Sabbioneda,S., Kannouche,P.L., Scott,A., Yasui,A., Green,C.M. and Lehmann,A.R. (2008) Regulation of proliferating cell nuclear antigen ubiquitination in mammalian cells. *Proc. Natl. Acad. Sci.*, **105**, 16125–16130.
52. Qin,Z., Lu,M., Xu,X., Hanna,M., Shiomi,N. and Xiao,W. (2013) DNA-damage tolerance mediated by PCNAUb fusions in human cells is dependent on Rev1 but not Polη. *Nucleic Acids Res.*, **41**, 7356–7369.
53. Le Beau,M.M., Rassool,F. V., Neilly,M.E., Espinosa,R., Glover,T.W., Smith,D.I. and McKeithan,T.W. (1998) Replication of a common fragile site, FRA3B, occurs late in S phase and is delayed further upon induction: Implications for the mechanism of fragile site induction. *Hum. Mol. Genet.*, **7**, 755–761.
54. Palakodeti,A., Lucas,I., Jiang,Y., Young,D.J., Fernald,A.A., Karrison,T. and Le Beau,M.M. (2009) Impaired replication dynamics at the FRA3B common fragile site. *Hum. Mol. Genet.*, **19**, 99–110.
55. Letessier,A., Millot,G.A., Koundrioukoff,S., Lachagès,A.M., Vogt,N., Hansen,R.S., Malfoy,B., Brison,O. and Debatisse,M. (2011) Cell-type-specific replication initiation programs set fragility of the FRA3B fragile site. *Nature*, **470**, 120–124.
56. Ozeri-Galai,E., Lebofsky,R., Rahat,A., Bester,A.C., Bensimon,A. and Kerem,B. (2011) Failure of Origin Activation in Response to Fork Stalling Leads to Chromosomal Instability at Fragile Sites. *Mol. Cell*, **43**, 122–131.
57. Kawabata,T., Luebben,S.W., Yamaguchi,S., Ilves,I., Matise,I., Buske,T., Botchan,M.R. and Shima,N. (2011) Stalled Fork Rescue via Dormant Replication Origins in Unchallenged S Phase Promotes Proper Chromosome Segregation and Tumor Suppression. *Mol. Cell*, **41**, 543–553.
58. Chan,K.L., Palmai-Pallag,T., Ying,S. and Hickson,I.D. (2009) Replication stress induces sister-chromatid bridging at fragile site loci in mitosis. *Nat. Cell Biol.*, **11**, 753–760.
59. Minocherhomji,S., Ying,S., Bjerregaard,V.A., Bursomanno,S., Aleliunaite,A., Wu,W., Mankouri,H.W., Shen,H., Liu,Y. and Hickson,I.D. (2015) Replication stress activates DNA repair synthesis in mitosis. *Nature*, **528**, 286–290.
60. Bhowmick,R., Minocherhomji,S. and Hickson,I.D. (2016) RAD52 Facilitates Mitotic DNA Synthesis Following Replication Stress. *Mol. Cell*, **64**, 1117–1126.
61. Graber-Feesl,C.L., Pederson,K.D., Aney,K.J. and Shima,N. (2019) Mitotic DNA synthesis is differentially regulated between cancer and noncancerous cells. *Mol. Cancer Res.*, **17**, 1687–1698.
62. Kim,H. and D'Andrea,A.D. (2012) Regulation of DNA cross-link repair by the Fanconi anemia/BRCA pathway. *Genes Dev.*, **26**, 1393–1408.
63. Thakar,T., Leung,W., Nicolae,C.M., Clements,K.E., Shen,B., Bielinsky,A.K. and Moldovan,G.L. (2020) Ubiquitinated-PCNA protects replication forks from DNA2-mediated degradation by regulating Okazaki fragment maturation and chromatin assembly. *Nat. Commun.*, **11**, 1–14.
64. Schlacher,K., Christ,N., Siaud,N., Egashira,A., Wu,H. and Jasin,M. (2011) Double-strand break repair-independent role for BRCA2 in blocking stalled replication fork degradation by MRE11. *Cell*, **145**, 529–542.
65. Schlacher,K., Wu,H. and Jasin,M. (2012) A Distinct Replication Fork Protection

Pathway Connects Fanconi Anemia Tumor Suppressors to RAD51-BRCA1/2. *Cancer Cell*, **22**, 106–116.
66. Couch,F.B., Bansbach,C.E., Driscoll,R., Luzwick,J.W., Glick,G.G., Bétous,R., Carroll,C.M., Jung,S.Y., Qin,J., Cimprich,K.A., *et al.* (2013) ATR phosphorylates SMARCAL1 to prevent replication fork collapse. *Genes Dev.*, **27**, 1610–1623.
67. Ying,S., Hamdy,F.C. and Helleday,T. (2012) Mre11-dependent degradation of stalled DNA replication forks is prevented by BRCA2 and PARP1. *Cancer Res.*, **72**, 2814–2821.
68. Nayak,S., Calvo,J.A., Cong,K., Peng,M., Berthiaume,E., Jackson,J., Zaino,A.M., Vindigni,A., Hadden,M.K. and Cantor,S.B. (2020) Inhibition of the translesion synthesis polymerase REV1 exploits replication gaps as a cancer vulnerability. *Sci. Adv.*, **6**, eaaz7808.
69. Simpson,L.J., Ross,A.L., Szüts,D., Alviani,C.A., Oestergaard,V.H., Patel,K.J. and Sale,J.E. (2006) RAD18-independent ubiquitination of proliferating-cell nuclear antigen in the avian cell line DT40. *EMBO Rep.*, **7**, 927–932.
70. Langerak,P., Nygren,A.O.H., Krijger,P.H.L., van den Berk,P.C.M. and Jacobs,H. (2007) A/T mutagenesis in hypermutated immunoglobulin genes strongly depends on PCNA ^{K164} modification. *J. Exp. Med.*, **204**, 1989–1998.
71. Forment,J. V. and Jackson,S.P. (2015) A flow cytometry-based method to simplify the analysis and quantification of protein association to chromatin in mammalian cells. *Nat. Protoc.*, **10**, 1297–1307.
72. Matson,J.P., Dumitru,R., Coryell,P., Baxley,R.M., Chen,W., Twaroski,K., Webber,B.R., Tolar,J., Bielinsky,A.K., Purvis,J.E., *et al.* (2017) Rapid DNA replication origin licensing protects stem cell pluripotency. *Elife*, **6**, 1–31.
73. Frampton,J., Irmisch,A., Green,C.M., Neiss,A., Trickey,M., Ulrich,H.D., Furuya,K., Watts,F.Z., Carr,A.M. and Lehmann,A.R. (2006) Postreplication Repair and PCNA Modification in Schizosaccharomyces pombe. *Mol. Biol. Cell*, **17**, 2976–2985.
74. Leach,C.A. and Michael,W.M. (2005) Ubiquitin/SUMO modification of PCNA promotes replication fork progression in Xenopus laevis egg extracts. *J. Cell Biol.*, **171**, 947–954.
75. Anglana,M., Apiou,F., Bensimon,A. and Debatisse,M. (2003) Dynamics of DNA replication in mammalian somatic cells: Nucleotide pool modulates origin choice and interorigin spacing. *Cell*, **114**, 385–394.
76. Poli,J., Tsaponina,O., Crabbé,L., Keszthelyi,A., Pantesco,V., Chabes,A., Lengronne,A. and Pasero,P. (2012) dNTP pools determine fork progression and origin usage under replication stress. *EMBO J.*, **31**, 883–894.
77. Zhong,Y., Nellimootti,T., Peace,J.M., Knott,S.R.V., Villwock,S.K., Yee,J.M., Jancuska,J.M., Rege,S., Tecklenburg,M., Sclafani,R.A., *et al.* (2013) The level of origin firing inversely affects the rate of replication fork progression. *J. Cell Biol.*, **201**, 373–383.
78. Rodriguez-Acebes,S., Mourón,S. and Méndez,J. (2018) Uncoupling fork speed and origin activity to identify the primary cause of replicative stress phenotypes. *J. Biol. Chem.*, **293**, 12855–12861.
79. Blow,J.J., Ge,X.Q. and Jackson,D.A. (2011) How dormant origins promote complete genome replication. *Trends Biochem. Sci.*, **36**, 405–414.
80. Luebben,S.W., Kawabata,T., Johnson,C.S., O'sullivan,M.G. and Shima,N. (2014) A

concomitant loss of dormant origins and FANCC exacerbates genome instability by impairing DNA replication fork progression. *Nucleic Acids Res.*, **42**, 5605–5615.
81. Alver,R.C., Chadha,G.S. and Blow,J.J. (2014) The contribution of dormant origins to genome stability: From cell biology to human genetics. *DNA Repair (Amst).*, **19**, 182–189.
82. Harrigan,J.A., Belotserkovskaya,R., Coates,J., Dimitrova,D.S., Polo,S.E., Bradshaw,C.R., Fraser,P. and Jackson,S.P. (2011) Replication stress induces 53BP1-containing OPT domains in G1 cells. *J. Cell Biol.*, **193**, 97–108.
83. Lukas,C., Savic,V., Bekker-Jensen,S., Doil,C., Neumann,B., Pedersen,R.S., Grøhfte,M., Chan,K.L., Hickson,I.D., Bartek,J., *et al.* (2011) 53BP1 nuclear bodies form around DNA lesions generated by mitotic transmission of chromosomes under replication stress. *Nat. Cell Biol.*, **13**, 243–253.
84. Moreno,A., Carrington,J.T., Albergante,L., Mamun,M. Al, Haagensen,E.J., Komseli,E.S., Gorgoulis,V.G., Newman,T.J. and Blow,J.J. (2016) Unreplicated DNA remaining from unperturbed S phases passes through mitosis for resolution in daughter cells. *Proc. Natl. Acad. Sci. U. S. A.*, **113**, E5757–E5764.
85. Lezaja,A. and Altmeyer,M. (2018) Inherited DNA lesions determine G1 duration in the next cell cycle. *Cell Cycle*, **17**, 24–32.
86. Ge,X.Q., Jackson,D.A. and Blow,J.J. (2007) Dormant origins licensed by excess Mcm2-7 are required for human cells to survive replicative stress. *Genes Dev.*, **21**, 3331–3341.
87. Ibarra,A., Schwob,E. and Méndez,J. (2008) Excess MCM proteins protect human cells from replicative stress by licensing backup origins of replication. *Proc. Natl. Acad. Sci. U. S. A.*, **105**, 8956–8961.
88. Alcón,P., Shakeel,S., Chen,Z.A., Rappsilber,J., Patel,K.J. and Passmore,L.A. (2020) FANCD2–FANCI is a clamp stabilized on DNA by monoubiquitination of FANCD2 during DNA repair. *Nat. Struct. Mol. Biol.*, **27**, 240–248.
89. Wang,R., Wang,S., Dhar,A., Peralta,C. and Pavletich,N.P. (2020) DNA clamp function of the monoubiquitinated Fanconi anaemia ID complex. *Nature*, **580**, 278–282.
90. Geng,L., Huntoon,C.J. and Karnitz,L.M. (2010) RAD18-mediated ubiquitination of PCNA activates the Fanconi anemia DNA repair network. *J. Cell Biol.*, **191**, 249–257.
91. Song,I.Y., Palle,K., Gurkar,A., Tateishi,S., Kupfer,G.M. and Vaziri,C. (2010) Rad18-mediated translesion synthesis of bulky DNA adducts is coupled to activation of the fanconi anemia DNA repair pathway. *J. Biol. Chem.*, **285**, 31525–31536.
92. Zhang,S., Chea,J., Meng,X., Zhou,Y., Lee,E.Y.C. and Lee,M.Y.W.T. (2008) PCNA is ubiquitinated by RNF8 ND SC RIB ND ES SC RIB. 10.4161/cc.7.21.6949.
93. Terai,K., Abbas,T., Jazaeri,A.A. and Dutta,A. (2010) CRL4Cdt2E3 Ubiquitin Ligase Monoubiquitinates PCNA to Promote Translesion DNA Synthesis. *Mol. Cell*, **37**, 143–149.
94. Roa,S., Avdievich,E., Peled,J.U., MacCarthy,T., Werling,U., Kuang,F.L., Kan,R., Zhao,C., Bergman,A., Cohen,P.E., *et al.* (2008) Ubiquitylated PCNA plays a role in somatic hypermutation and class-switch recombination and is required for meiotic progression. *Proc. Natl. Acad. Sci.*, **105**, 16248–16253.
95. Pilzecker,B., Buoninfante,O.A., Van Den Berk,P., Lancini,C., Song,J.Y., Citterio,E.

and Jacobs,H. (2017) DNA damage tolerance in hematopoietic stem and progenitor cells in mice. *Proc. Natl. Acad. Sci. U. S. A.*, **114**, E6875–E6883.
96. Parmar,K., D'Andrea,A. and Niedernhofer,L.J. (2009) Mouse models of Fanconi anemia. *Mutat. Res. - Fundam. Mol. Mech. Mutagen.*, **668**, 133–140.
97. Bakker,S.T., De Winter,J.P. and Te Riele,H. (2013) Learning from a paradox: Recent insights into Fanconi anaemia through studying mouse models. *DMM Dis. Model. Mech.*, **6**, 40–47.
98. Pagès,V., Johnson,R.E., Prakash,L. and Prakash,S. (2008) Mutational specificity and genetic control of replicative bypass of an abasic site in yeast. *Proc. Natl. Acad. Sci. U. S. A.*, **105**, 1170–1175.
99. Yoon,J.H., Prakash,L. and Prakash,S. (2009) Highly error-free role of DNA polymerase η in the replicative bypass of UV-induced pyrimidine dimers in mouse and human cells. *Proc. Natl. Acad. Sci. U. S. A.*, **106**, 18219–18224.
100. Yoon,J.H., Prakash,S. and Prakash,L. (2012) Genetic control of translesion synthesis on leading and lagging DNA strands in plasmids derived from epstein-barr virus in human cells. *MBio*, **3**, 1–7.
101. Hedglin,M. and Benkovic,S.J. (2017) Eukaryotic Translesion DNA Synthesis on the Leading and Lagging Strands: Unique Detours around the Same Obstacle. *Chem. Rev.*, **117**, 7857–7877.
102. Taylor,M.R.G. and Yeeles,J.T.P. (2018) The Initial Response of a Eukaryotic Replisome to DNA Damage. *Mol. Cell*, **70**, 1067-1080.e12.
103. Taylor,M.R.G. and Yeeles,J.T.P. (2019) Dynamics of Replication Fork Progression Following Helicase–Polymerase Uncoupling in Eukaryotes. *J. Mol. Biol.*, **431**, 2040–2049.
104. Guilliam,T.A. and Yeeles,J.T.P. (2020) Reconstitution of translesion synthesis reveals a mechanism of eukaryotic DNA replication restart. *Nat. Struct. Mol. Biol.*, **27**, 450–460.
105. Garcia-Exposito,L., Bournique,E., Bergoglio,V., Bose,A., Barroso-Gonzalez,J., Zhang,S., Roncaioli,J.L., Lee,M., Wallace,C.T., Watkins,S.C., *et al.* (2016) Proteomic Profiling Reveals a Specific Role for Translesion DNA Polymerase η in the Alternative Lengthening of Telomeres. *Cell Rep.*, **17**, 1858–1871.
106. Bergoglio,V., Boyer,A.S., Walsh,E., Naim,V., Legube,G., Lee,M.Y.W.T., Rey,L., Rosselli,F., Cazaux,C., Eckert,K.A., *et al.* (2013) DNA synthesis by pol η promotes fragile site stability by preventing under-replicated DNA in mitosis. *J. Cell Biol.*, **201**, 395–408.
107. Maya-Mendoza,A., Moudry,P., Merchut-Maya,J.M., Lee,M., Strauss,R. and Bartek,J. (2018) High speed of fork progression induces DNA replication stress and genomic instability. *Nature*, **559**, 279–284.
108. Das-Bradoo,S., Nguyen,H.D., Wood,J.L., Ricke,R.M., Haworth,J.C. and Bielinsky,A.K. (2010) Defects in DNA ligase i trigger PCNA ubiquitylation at Lys 107. *Nat. Cell Biol.*, **12**, 74–79.
109. Nguyen,H.D., Becker,J., Thu,Y.M., Costanzo,M., Koch,E.N., Smith,S., Myung,K., Myers,C.L., Boone,C. and Bielinsky,A.K. (2013) Unligated Okazaki Fragments Induce PCNA Ubiquitination and a Requirement for Rad59-Dependent Replication Fork Progression. *PLoS One*, **8**.
110. Becker,J.R., Pons,C., Nguyen,H.D., Costanzo,M., Boone,C., Myers,C.L. and

Bielinsky,A.K. (2015) Genetic Interactions Implicating Postreplicative Repair in Okazaki Fragment Processing. *PLoS Genet.*, **11**, 1–24.
111. Ticau,S., Friedman,L.J., Ivica,N.A., Gelles,J. and Bell,S.P. (2015) Single-molecule studies of origin licensing reveal mechanisms ensuring bidirectional helicase loading. *Cell*, **161**, 513–525.
112. Hanzlikova,H., Kalasova,I., Demin,A.A., Pennicott,L.E., Cihlarova,Z. and Caldecott,K.W. (2018) The Importance of Poly(ADP-Ribose) Polymerase as a Sensor of Unligated Okazaki Fragments during DNA Replication. *Mol. Cell*, **71**, 319-331.e3.
113. Sriramachandran,A.M., Petrosino,G., Méndez-Lago,M., Schäfer,A.J., Batista-Nascimento,L.S., Zilio,N. and Ulrich,H.D. (2020) Genome-wide Nucleotide-Resolution Mapping of DNA Replication Patterns, Single-Strand Breaks, and Lesions by GLOE-Seq. *Mol. Cell*, 10.1016/j.molcel.2020.03.027.
114. Spies,J., Lukas,C., Somyajit,K., Rask,M.B., Lukas,J. and Neelsen,K.J. (2019) 53BP1 nuclear bodies enforce replication timing at under-replicated DNA to limit heritable DNA damage. *Nat. Cell Biol.*, **21**, 487–497.
115. Hussain,S., Wilson,J.B., Medhurst,A.L., Hejna,J., Witt,E., Ananth,S., Davies,A., Masson,J.Y., Moses,R., West,S.C., *et al.* (2004) Direct interaction of FANCD2 with BRCA2 in DNA damage response pathways. *Hum. Mol. Genet.*, **13**, 1241–1248.
116. Howlett,N.G., Taniguchi,T., Durkin,S.G., D'Andrea,A.D. and Glover,T.W. (2005) The Fanconi anemia pathway is required for the DNA replication stress respone and for the regulation of common fragile site stability. *Hum. Mol. Genet.*, **14**, 693–701.
117. Howlett,N.G., Harney,J.A., Rego,M.A., Kolling IV,F.W. and Glover,T.W. (2009) Functional interaction between the fanconi anemia D2 protein and proliferating cell nuclear antigen (PCNA) via a conserved putative PCNA interaction motif. *J. Biol. Chem.*, **284**, 28935–28942.
118. Rego,M.A., Kolling IV,F.W., Vuono,E.A., Mauro,M. and Howlett,N.G. (2012) Regulation of the Fanconi anemia pathway by a CUE ubiquitin-binding domain in the FANCD2 protein. *Blood*, **120**, 2109–2117.
119. Meetei,A.R., De Winter,J.P., Medhurst,A.L., Wallisch,M., Waisfisz,Q., Van de Vrugt,H.J., Oostra,A.B., Yan,Z., Ling,C., Bishop,C.E., *et al.* (2003) A novel ubiquitin ligase is deficient in Fanconi anemia. *Nat. Genet.*, **35**, 165–170.
120. Alpi,A.F., Pace,P.E., Babu,M.M. and Patel,K.J. (2008) Mechanistic Insight into Site-Restricted Monoubiquitination of FANCD2 by Ube2t, FANCL, and FANCI. *Mol. Cell*, **32**, 767–777.
121. Song,I.Y., Barkley,L.R., Day,T.A., Weiss,R.S. and Vaziri,C. (2010) A novel role for fanconi anemia (FA) pathway effector protein FANCD2 in cell cycle progression of untransformed primary human cells. *Cell Cycle*, **9**, 2375–2388.
122. Ran,F.A., Hsu,P.D., Wright,J., Agarwala,V., Scott,D.A. and Zhang,F. (2013) Genome engineering using the CRISPR-Cas9 system. *Nat Protoc*, **8**, 2281–2308.
123. Fattah,F.J., Kweon,J., Wang,Y., Lee,E.H., Kan,Y., Lichter,N., Weisensel,N. and Hendrickson,E.A. (2014) A role for XLF in DNA repair and recombination in human somatic cells. *DNA Repair*, **15**, 39–53.
124. Kohli,M., Rago,C., Lengauer,C., Kinzler,K.W. and Vogelstein,B. (2004) Facile methods for generating human somatic cell gene knockouts using recombinant

adeno-associated viruses. *Nucleic Acids Res*, **32**, e3.
125. Oh,S., Harvey,A., Zimbric,J., Wang,Y., Nguyen,T., Jackson,P.J. and Hendrickson,E.A. (2014) DNA ligase III and DNA ligase IV carry out genetically distinct forms of end joining in human somatic cells. *DNA Repair*, **21**, 97–110.
126. Thompson,E.L., Yeo,J.E., Lee,E.A., Kan,Y., Raghunandan,M., Wiek,C., Hanenberg,H., Schärer,O.D., Hendrickson,E.A. and Sobeck,A. (2017) FANCI and FANCD2 have common as well as independent functions during the cellular replication stress response. *Nucleic Acids Res.*, **45**, 11837–11857.
127. Brinkman,E.K., Chen,T., Amendola,M. and Van Steensel,B. (2014) Easy quantitative assessment of genome editing by sequence trace decomposition. *Nucleic Acids Res.*, **42**.
128. Becker,J.R., Gallo,D., Leung,W., Croissant,T., Thu,Y.M., Nguyen,H.D., Starr,T.K., Brown,G.W. and Bielinsky,A.-K. (2018) Flap endonuclease overexpression drives genome instability and DNA damage hypersensitivity in a PCNA-dependent manner. *Nucleic Acids Res.*, **46**, 5634–5650.

ACKNOWLEDGEMENTS

We would like to thank the University of Minnesota Flow Cytometry Core Facility, Imaging Center and Cytogenomics Shared Resource.

AUTHOR CONTRIBUTIONS

Conceptualization, A.K.B. and W.L.; Methodology, A.K.B., W.L., N.S.; Formal Analysis, A.K.B., W.L.; Investigation, W.L., R.M.B., T.T., J.P.B., L.W., C.B.R., A.T.; Writing – Original Draft, W.L., and A.K.B.; Writing – Review & Editing, W.L., R.M.B., A.K.B., G.L.M., N.S.; Visualization, W.L., Supervision, A.K.B., Project Administration, W.L. and A.K.B.; Funding Acquisition, A.K.B.

FUNDING

This work was supported by: National Institutes of General Medicine Sciences [NIGMS R01-GM 074917 to A.K.B. and R01-GM134681 to A.K.B. and G.L.M.], National Cancer Institute [NCI T32-CA009138 to W.L. R.M.B. and C.B.R.], and the ARCS Foundation [C.B.R.].

DECLARATION OF INTEREST

The authors declare no competing interests.

FIGURE TITLES AND LEGENDS

Figure 1. *PCNA^{K164R}* mutant cell lines exhibit increased sensitivity to DNA damage

A) Chromatin associated PCNA, ubiquityl-PCNA (K164), phospho-RPA32 (S4/8), and γH2AX, with or without 20J/m^2 and 40J/m^2 UV treatment, with histone H2AX as the loading control. Quantification of Ub-PCNA, K164-Ub PCNA, phospho-RPA32, and γH2AX levels normalized to loading control.

B) Western blot analyses of whole cell extracts from wildtype RPE-1 and *PCNA^{K164R}* cells for phospho-p53 (S15), p53, and p21 with or without 10J/m^2 and 40J/m^2 UV treatment, with GAPDH as the loading control. Quantification of phosphor-p53 (S15), p53, and p21 levels normalized to loading control.

C) Comparison of drug sensitivity as measured by MTS assay comparing average percent viability in RPE-1 wildtype and *PCNA^{K164R}* cell lines. Each drug and concentration tested is indicated. Error bars indicate standard deviation and statistical significance was calculated using students *t-test* with *>.05; **>.01, ***>.001; n=9 replicate wells across three biological replicates for all data points.

D) Representative cell cycle distribution of RPE-1 wildtype and *PCNA^{K164R}* cell lines treated with or without MMS (10 uM) and MMC (20 nM) for 48 h, based on DNA content (PI).

E) Cell cycle distribution of RPE-1 wildtype and *PCNA^{K164R}* cell lines treated with or without MMS and MMC from three biological replicates. Percent of each population in G1- (green), S- (purple) or G2/M-phase (gray) is shown.

Figure 2. The PCNA-K164R mutation causes significant cell cycle and DNA synthesis defects

A) Average cell proliferation rate in *PCNA*^{K164R} cell lines normalized to wildtype. For each cell line n=9 wells across three biological replicates. Error bars indicate standard deviation and significance was calculated using students *t-test* with *>.05; **>.01, ***>.001.

B) Representative flow cytometry plots sorting cells based on propidium iodide and annexin V staining for the quantification of early apoptotic, late apoptotic and dead cells in RPE-1 wildtype and *PCNA*^{K164R} cell lines.

C) Percent of each population represented by early apoptotic, late apoptotic or dead cells. Error bars indicate standard deviation and significance was calculated using students *t-test* with *>.05; **>.01, ***>.001; n=6 replicates across two biological replicates.

D) Representative cell cycle distribution of RPE-1 wildtype and *PCNA*^{K164R} cell lines based on DNA content (DAPI) and DNA synthesis (EdU incorporation). Percent of each population in G1- (green), S- (purple) or G2/M-phase (gray) is shown. Asterisks indicate tetraploid lines.

E) Cell cycle distribution of RPE-1 wildtype and *PCNA*^{K164R} cell lines from three biological replicates. Percent of each population in G1- (green), S- (purple) or G2/M-phase (gray) is shown. Error bars indicate standard deviation and significance was calculated using students *t-test* with *>.05; **>.01, ***>.001.

F) Histogram (left) and quantification of mean fluorescent intensity (right) of EdU staining of S-phase cells from RPE-1 wildtype (blue) and *PCNA*^{K164R} cells (maroon); n=9 across three biological replicates. Error bars indicate standard deviation and significance was calculated using students *t-test* with *>.05; **>.01, ***>.001.

Figure 3. Defects in DNA synthesis in RPE-1 *PCNA*^{K164R} cells are caused by reduced origin licensing

A) Schematic of quantitative chromatin flow cytometry analysis. Cell cycle phase is defined by DNA content, EdU incorporation and chromatin loaded MCM2.

B) Representative chromatin flow cytometry plots for RPE-1 wildtype and *PCNA*^{K164R} cells. G1-phase/MCM positive cells (blue), S-phase/MCM positive cells (orange) and G1- or G2/M-phase/MCM negative cells (gray) are indicated. Asterisks indicate tetraploid lines.

C) Representative chromatin flow cytometry density plots for RPE-1 wildtype and *PCNA*^{K164R} cells. Percentage of MCM2 stained cells in late G1 is indicated (red box). Asterisks indicate tetraploid lines.

D) Quantification of mean fluorescent intensity of MCM2 staining of G1 cells from RPE-1 wildtype (blue) and *PCNA*^{K164R} cells (maroon); n=9 across three biological replicates. Error bars indicate standard deviation and significance was calculated using students *t-test* with *>.05; **>.01, ***>.001.

E) Quantification of the percentage of MCM2 stained cells in late G1 from RPE-1 wildtype (blue) and *PCNA*^{K164R} cells (maroon); n=3 across three biological replicates. Error bars

indicate standard deviation and significance was calculated using students *t-test* with *>.05; **>.01; ***>.001.

Figure 4. *PCNA^{K164R}* mutants display DNA replication defects and accumulate under-replicated DNA

A) Example DNA fibers used for DNA combing analyses. Active replication forks were sequentially labeled with IdU (25 μM, green) for 30 minutes followed by labeling with CldU (200 μM, red) for 30 minutes. Inter-origin distance (IOD) is measured as center to center distance between two adjacent progressing bidirectional forks. Green arrows represent the direction of fork progression. New origin firing (NOF) is measured as CldU-only tracts. Fork speed is calculated by dividing the length of the CldU track by the time of the pulse. All quantifications (B-E) were obtained under unperturbed conditions.

B) IOD quantification from three biological replicates in wildtype (blue) and *PCNA^{K164R}* cells (maroon). Average IOD and number (n) quantified is listed. Significance was calculated by Mann-Whitney Ranked Sum Test with *>.05; **>.01; ***>.001.

C) New origin firing (NOF) events from 5 biological replicates in RPE-1 wildtype (blue) and *PCNA^{K164R}* 1E12, 2B10 (maroon). NOF events from 3 biological replicates in *PCNA$^{K164R/-}$ 1E4* (maroon). Number (n) of events quantified is listed. Significance was calculated using students *t-test* with *>.05, **>0.01.

D) Fork speed from three biological replicates in RPE-1 wildtype (blue) and *PCNA^{K164R}* cells (maroon). Average fork speed and number (n) quantified is listed. Significance was calculated by Mann-Whitney Ranked Sum Test with *>.05; **>.01; ***>.001.

E) Fork stability from three biological replicates in RPE-1 wildtype (blue) and *PCNA*^{K164R} cells (maroon). Average fork stability and number (n) quantified is listed. Significance was calculated by Mann-Whitney Ranked Sum Test with *>.05; **>.01; ***>.001.

F) (Left) Image of 53BP1 NB and cyclin A staining in RPE-1 cell lines. DAPI (blue), 53BP1 NB (green), and cyclin A (pink) are indicated. Scale bar at 20 μm. (Right) 53BP1 NB quantification of untreated (circles) and APH treated (triangles) in wildtype (blue) and *PCNA*^{K164R} lines (maroon). Number (n) of nuclei quantified is listed. Error bars indicate standard deviation and significance was calculated using one-way analysis of variance (ANOVA) with Tukey's multiple comparison test with ***<.001.

Figure 5. PCNA-K164 ubiquitination regulates MiDAS through the mono-ubiquitination of FANCD2

A) Representative images of phospho-H3-stained nuclei/chromosomes (blue), EdU foci (green), and FANCD2 (red) foci for each RPE-1 cell line. Scale bars are 5 μm.

B) FANCD2 foci quantification from two biological replicates in RPE-1 wildtype (blue), *RAD18*$^{-/-}$ (pink), *PCNA*^{K164R} (maroon), and *RAD18*$^{-/-}$*PCNA*^{K164R} (purple) cells treated with APH. Number (n) of nuclei quantified is listed. Significance was calculated by one-way analysis of variance (ANOVA) with Tukey's multiple comparison test with ***<.001.

C) EdU foci quantification from two biological replicates in RPE-1 wildtype (blue), *RAD18*$^{-/-}$ (pink), *PCNA*^{K164R} (maroon), and *RAD18*$^{-/-}$*PCNA*^{K164R} (purple) cells treated with APH. Number (n) of nuclei quantified is listed. Significance was calculated by one-way analysis of variance (ANOVA) with Tukey's multiple comparison test with ***<.001.

D) FANCD2 foci quantification from two biological replicates in 293T wildtype (blue) and *PCNA*^{K164R} cells complemented with either wildtype (orange) or a K164R (red) cDNA treated with APH. Number (n) of nuclei quantified is listed. Significance was calculated by one-way analysis of variance (ANOVA) with Tukey's multiple comparison test with ***<.001.

E) EdU foci quantification from two biological replicates in 293T wildtype (blue) and *PCNA*^{K164R} cells complemented with either wildtype (orange) or a K164R (red) cDNA treated with APH. Number (n) of nuclei quantified is listed. Significance was calculated by one-way analysis of variance (ANOVA) with Tukey's multiple comparison test with ***<.001.

F) (Top) Chromatin associated FANCD2 with Ku86 as the loading control in RPE-1 wildtype and *PCNA*^{K164R} cell lines. Ratio of mono-ubiquitinated to non-ubiquitinated FANCD2 is indicated. (Bottom) Western blot analyses of whole cell extracts from RPE-1 wildtype and *PCNA*^{K164R} cell lines for FANCD2 with GAPDH as the loading control. Quantification of total FANCD2 levels normalized to loading control.

G) (Top) Chromatin associated FANCD2 with Ku86 as the loading control in 293T wildtype and *PCNA*^{K164R} cells complemented with either wildtype or a K164R cDNA. Ratio of mono-ubiquitinated to non-ubiquitinated FANCD2 is indicated. (Bottom) Western blot analyses of whole cell extracts from 293T wildtype and *PCNA*^{K164R} cells complemented with either wildtype or a K164R cDNA for FANCD2 with GAPDH as the loading control. Quantification of total FANCD2 levels normalized to loading control.

Figure 6. Absence of PCNA-K164 ubiquitination leads to under-licensing and defects in MiDAS

Wildtype (Left): PCNA K164-ubiquitination occurs during normal S-phase to promote gap filling of Okazaki fragments. If the replication fork encounters a DNA lesion/impediment, cells can still complete replication by activating DDT pathways. DNA that is not fully duplicated before G2/M stimulates MiDAS activation through the recruitment of FANCD2. In the subsequent G1 phase, origins are loaded and licensed in excess prior to S-phase. *PCNA*^{K164R} (Right): During S-phase, in the absence of PCNA K164-ubiquitination, Okazaki fragment ligation by LIG1 is impaired, which leads to the accumulation of ssDNA gaps. In the presence of a DNA lesion/impediment, DDT pathway activation does not occur, and the replication fork stalls. These defects result in a high frequency of under-replicated DNA. These under-replicated regions will eventually succumb to breakage, as MiDAS is severely compromised. In the subsequent G1 phase, an insufficient number of origins are assembled and licensed due to the accumulation of ssDNA gaps from the previous S-phase.

Figure S1. Generation of a *PCNA*^{K164R} mutant cell line in RPE-1 using CRISPR/Cas9

A) Schematic of the human *PCNA* indicating that exon 5 was targeted by CRISPR-Cas9. The K164R mutation was knocked-in utilizing a donor plasmid.

B) Schematic of screening PCR and expected PCR product sizes after EcoRI restriction enzyme digestion.

C) Representative genotyping PCR. Not targeted (wildtype; 1426 bp), monoallelic knock-in (KIN) (*PCNA*$^{KR/-}$ 1E4; 1426 bp, 1168 bp, 258 bp), and biallelic KIN (*PCNA*$^{KR/KR}$ 1E12, 2B10; 1168bp, 258 bp).

D) Karyotyping analysis from RPE-1 wildtype, *PCNA*$^{KR/KR}$ (1E12, 2B10) and *PCNA*$^{KR/-}$ (1E4) cell lines. Blue indicates expected RPE-1 karyotype. Red indicates chromosomal abnormalities.

E) Western blot analyses of whole cell extracts from wildtype RPE-1, *PCNA*^{K164R}, and *RAD18*$^{-/-}$ cells for MCM2 with α-Tubulin as the loading control. Quantification of MCM2 levels normalized to loading control.

Figure S2. 293T *PCNA*^{K164R} mutant cells exhibit significant DNA synthesis defects

A) Average cell proliferation rate in 293T *PCNA*^{K164R} lines complemented with either wildtype or K164R cDNA normalized to wildtype. For each cell line, n=9 wells across three biological replicates. Error bars indicate standard deviation and significance was calculated using students *t-test* with **>.01.

B) Representative cell cycle distribution of 293T wildtype and *PCNA*^{K164R} lines complemented with either wildtype or K164R cDNA based on DNA content (DAPI) and DNA synthesis (EdU incorporation). Percent of each population in G1- (green), S- (purple) or G2/M-phase (gray) is shown.

C) Cell cycle distribution of 293T wildtype and *PCNA*^{K164R} lines complemented with either wildtype or K164R cDNA from three biological replicates. Percent of each population in G1- (green), S- (purple) or G2/M-phase (gray) is shown. Error bars indicate standard deviation and significance was calculated using students *t-test* with ***>.001.

Please note that EdU incorporation reported by Thakar *et al.* (63) was performed using different experimental conditions.

D) Histogram (left) and quantification of mean fluorescent intensity (right) of EdU staining of S-phase cells from 293T wildtype (blue) and *PCNA*^{K164R} lines complemented with either wildtype (orange) or K164R (red) cDNA, n=9 across three biological replicates. Error bars indicate standard deviation and significance was calculated using students *t-test* with *>.05.

Figure S3. Reduced MCM2 loading in 293T *PCNA*^{K164R} cells

A) Representative chromatin flow cytometry plots for 293T wildtype, *PCNA*^{K164R} cells complemented with either wildtype PCNA or a K164R cDNA. G1-phase/MCM positive cells (blue), S-phase/MCM positive cells (orange) and G1- or G2/M-phase/MCM negative cells (gray) are indicated.

B) Quantification of mean fluorescent intensity of MCM2 staining of G1 cells from 293T wildtype (blue) and *PCNA*^{K164R} cells complemented with either wildtype (orange) or a K164R (red) cDNA; n=6 across two biological replicates. Error bars indicate standard deviation and significance was calculated using students *t-test* with *>.05.

C) Representative chromatin flow cytometry density plots for 293T wildtype, *PCNA*^{K164R} cells complemented with either wildtype or a K164R cDNA. Percentage of MCM2 stained cells in late G1 is indicated (red box).

D) Quantification of the percentage of MCM2 stained cells in late G1 from 293T wildtype (blue) and *PCNA*^{K164R} cells complemented with wildtype (orange) or a K164R (red)

cDNA; n=3 across three biological replicates. Error bars indicate standard deviation and significance was calculated using students *t-test* with *>.05.

Figure S4. Replication defects in 293T *PCNA^{K164R}* cells

A) Active replication forks were sequentially labeled with IdU (100 μM, green) for 15 minutes followed by labeling with CldU (100 μM, red) for 15 minutes. NOF is measured as CldU-only tracts. NOF events under unperturbed conditions from 2 biological replicates in 293T *PCNA^{K164R}* lines complemented with either wildtype (orange) or K164R (red) cDNA normalized to wildtype. Number (n) of events quantified is listed. Significance was calculated using students *t-test* with *>.05.

B) 53BP1 NB quantification of untreated (circles) and APH treated (triangles) 293T wildtype (blue) and *PCNA^{K164R}* lines complemented with either wildtype (orange) or K164R (red) cDNA. Number (n) of nuclei quantified is listed. Error bars indicate standard deviation and significance was calculated using one-way analysis of variance (ANOVA) with Tukey's multiple comparison test with ***<.001.

Figure S5. Enhanced MiDAS activation in MCM4 knockdown cells

A) Western blot analyses of whole cell extracts from wildtype RPE-1 cells treated with siControl or siMCM4 for MCM2, MCM3, MCM4, and MCM7 with α-Tubulin as the loading control.

B) FANCD2 foci quantification from two biological replicates in wildtype RPE-1 cells treated with siControl (blue) or siMCM4 (purple). Number (n) of nuclei quantified is listed. Significance was calculated by students *t-test* with ***<.001.

C) EdU foci quantification from two biological replicates in wildtype RPE-1 cells treated with siControl (blue) or siMCM4 (purple). Number (n) of nuclei quantified is listed. Significance was calculated by students *t-test* with ***<.001.

Figure S6. Reduced FANCD2 and EdU foci in *PCNA*^{K164R} mutants

A) Bins of 0, 1-9, 10-19 and >20 FANCD2 foci and EdU foci per nucleus from two biological replicates of RPE-1 wildtype (blue), *RAD18*$^{-/-}$ (pink), *PCNA*^{K164R} (maroon), and *RAD18*$^{-/-}$*:PCNA*^{K164R} (purple) cells.

B) Bins of 0, 1-9, 10-19 and >20 FANCD2 foci and EdU foci per nucleus from two biological replicates in 293T wildtype (blue) and *PCNA*^{K164R} cells complemented with either wildtype (orange) or a K164R (red) cDNA.

Figure 1. *PCNA*^{K164R} mutant cell lines exhibit increased sensitivity to DNA damage

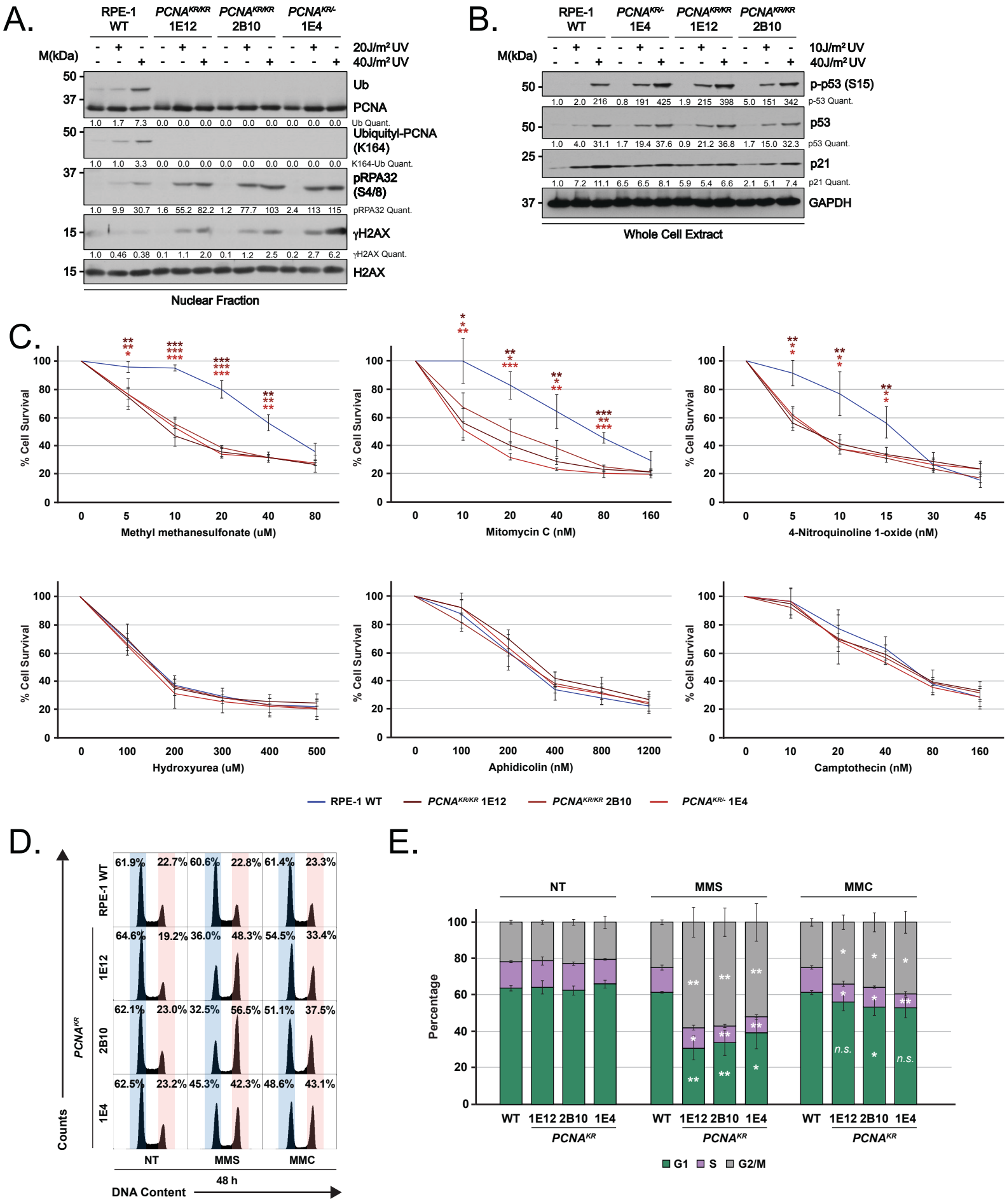

Figure 2. The PCNA-K164R mutation causes significant cell cycle and DNA synthesis defects

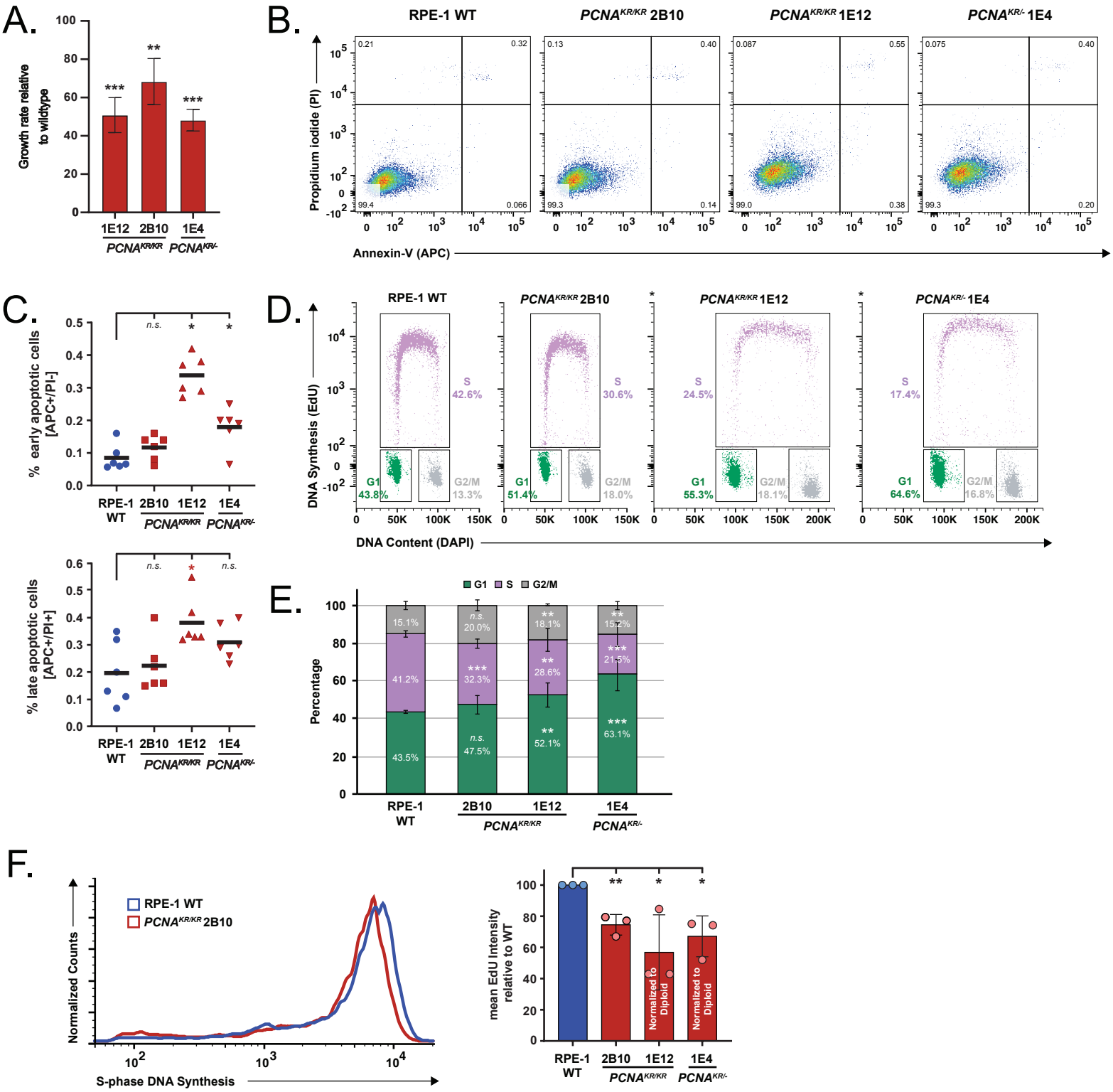

Figure 3. Defects in DNA synthesis in RPE-1 *PCNA*^{K164R} cells are caused by reduced origin licensing

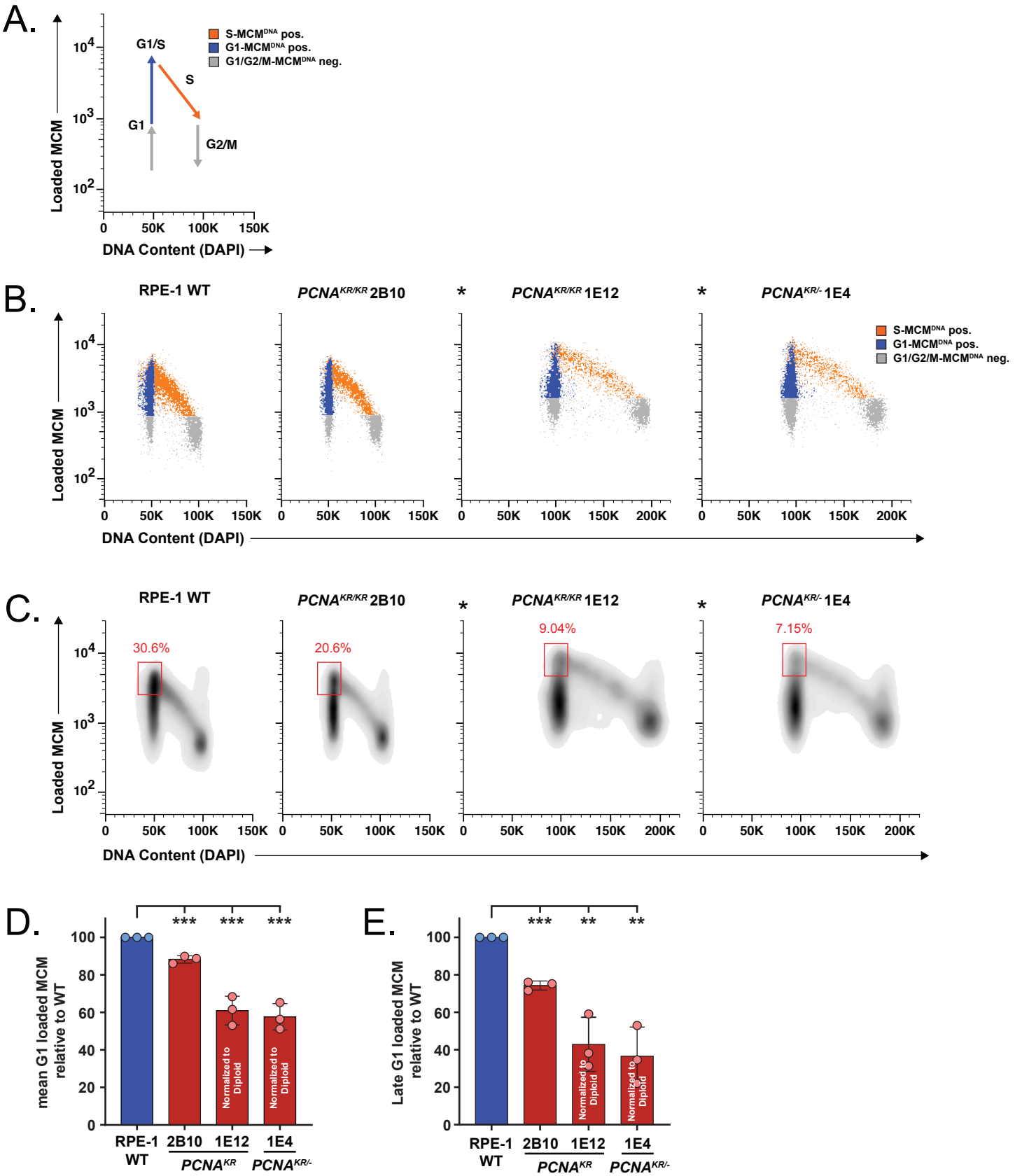

Figure 4. *PCNA*^{K164R} mutant cells display DNA replication defects and accummulate under-replicated DNA

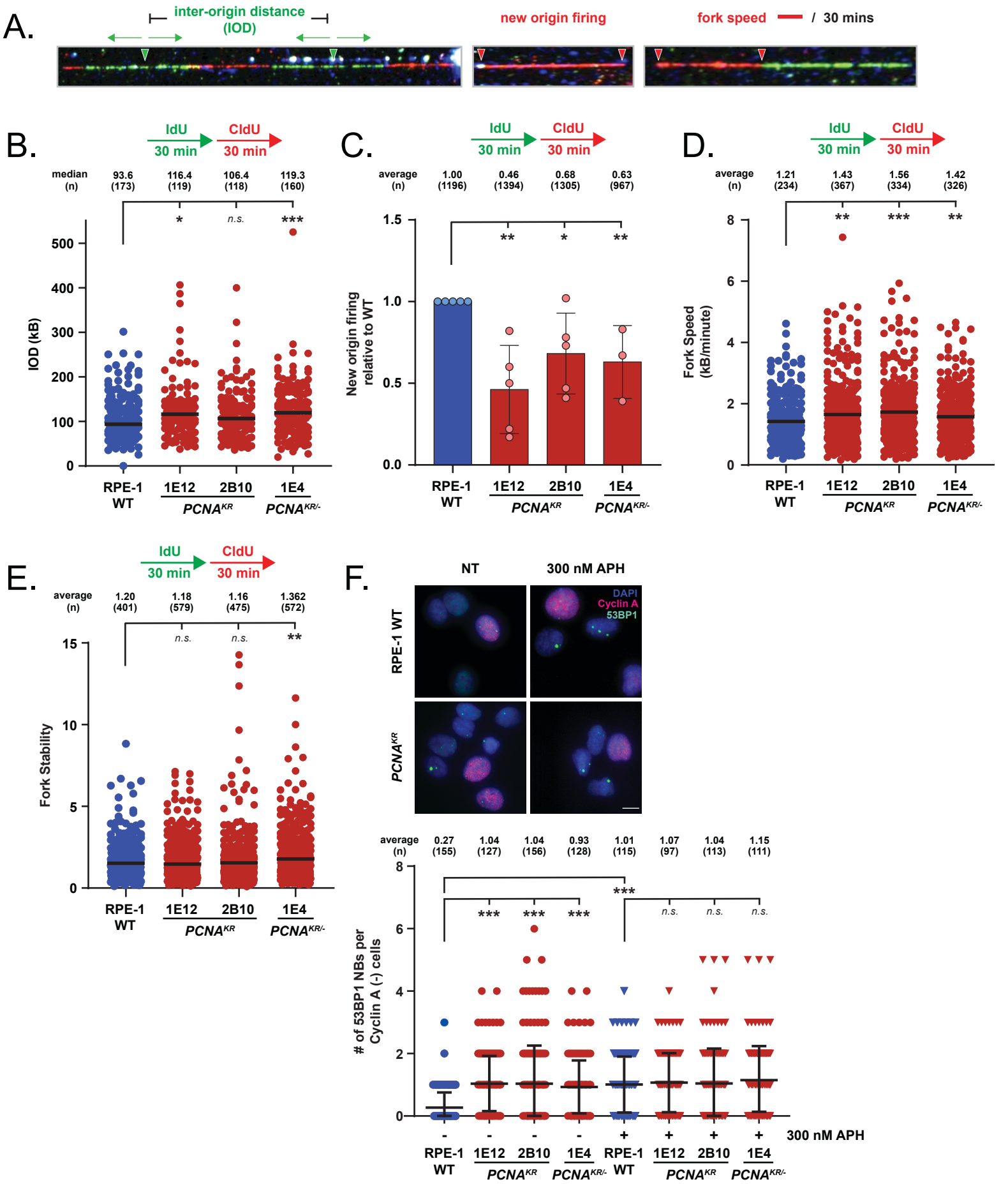

Figure 5. PCNA-K164 ubiquitination regulates MiDAS through the mono-ubiquitination of FANCD2

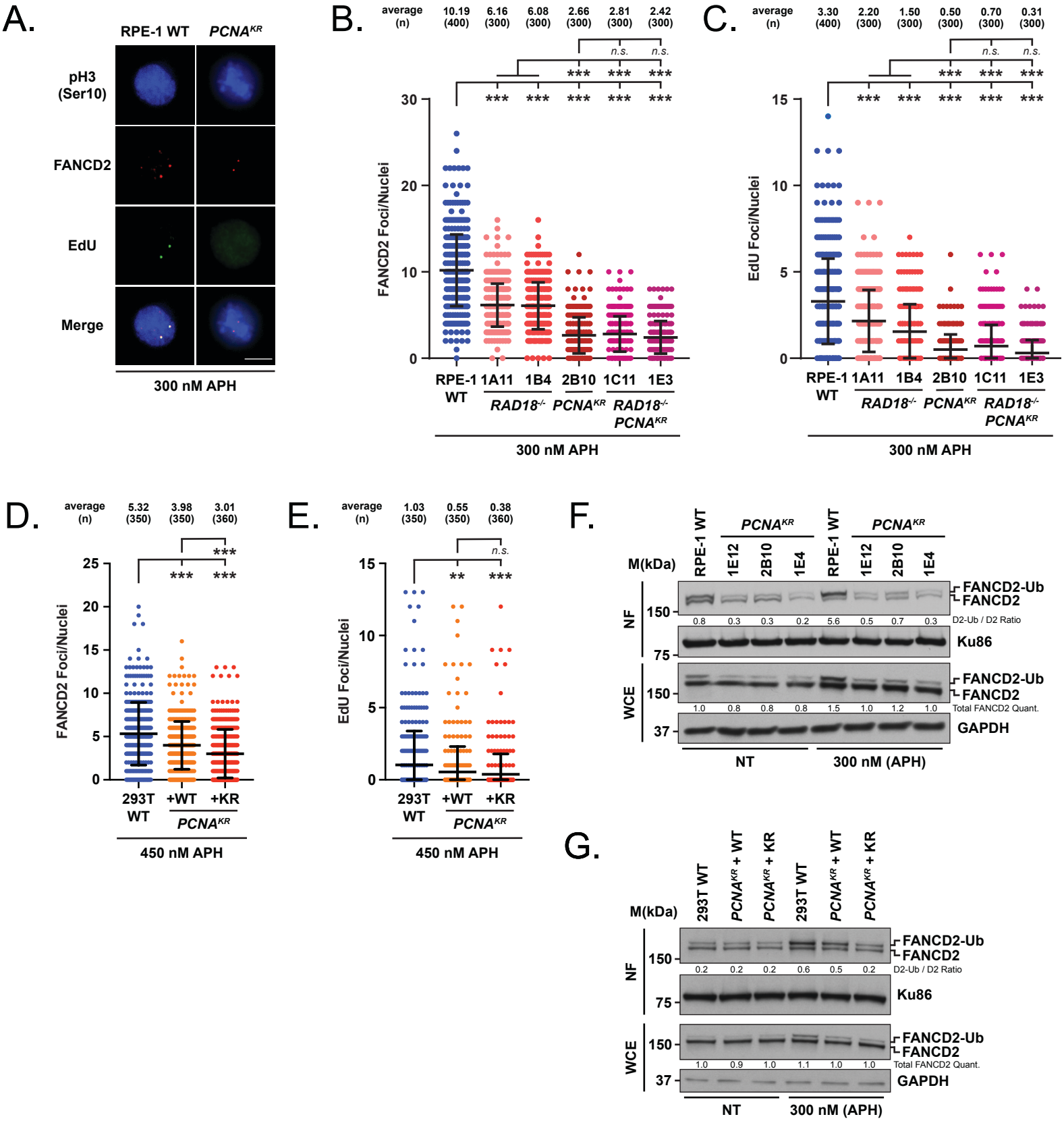

Figure 6. Absence of PCNA K164 ubiquitination leads to under-licensing and defects in MiDAS

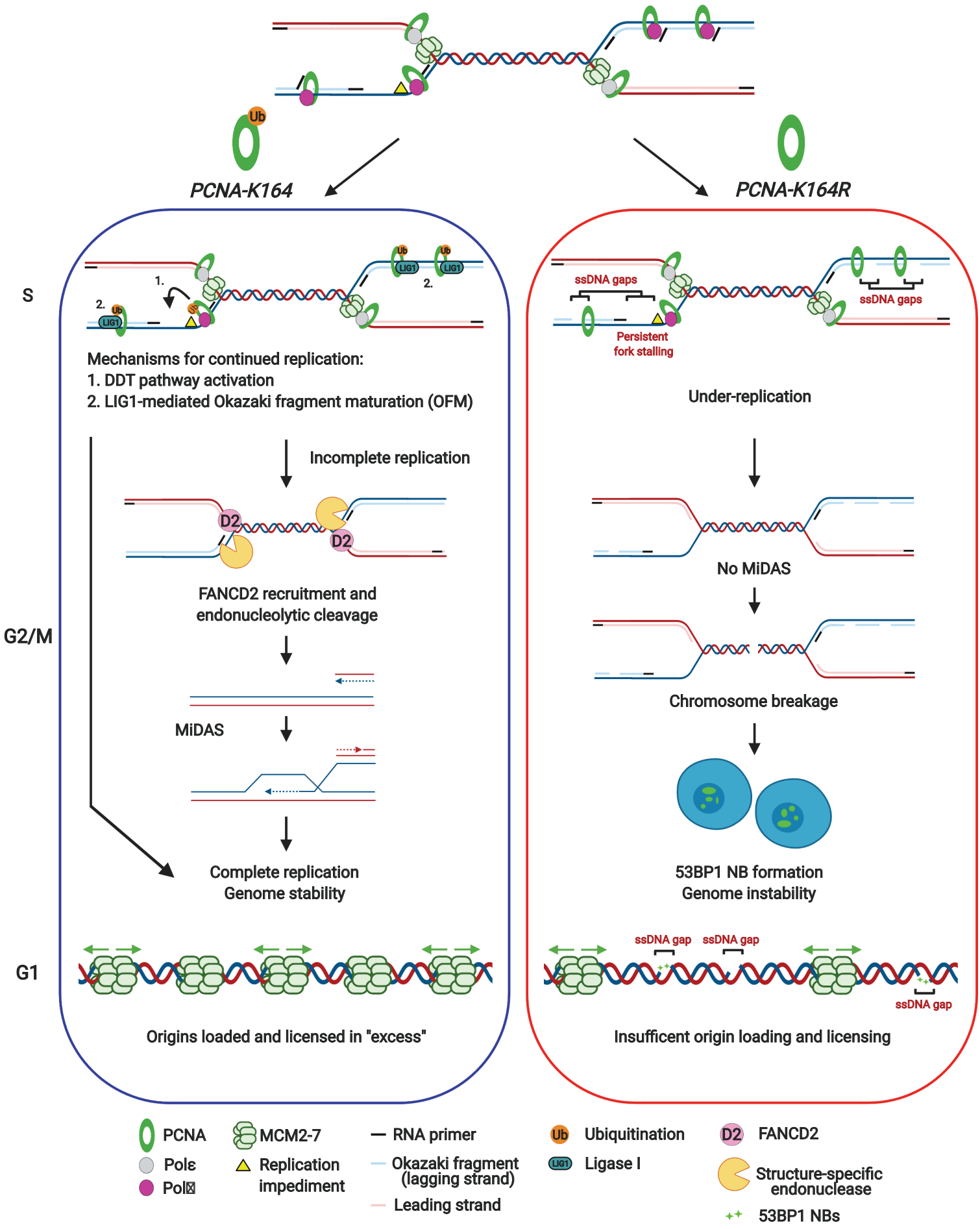

Figure S1. Generation of a *PCNA*^{K164R} mutant cell line in hTERT RPE-1 using CRISPR-Cas9

A.

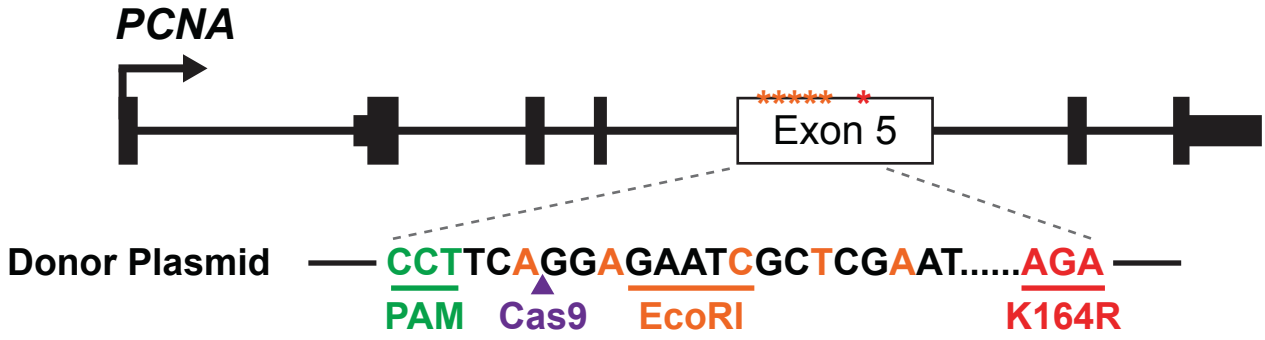

B.

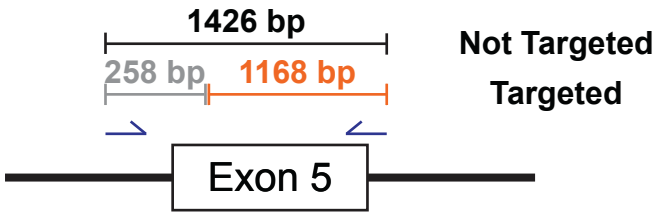

C.

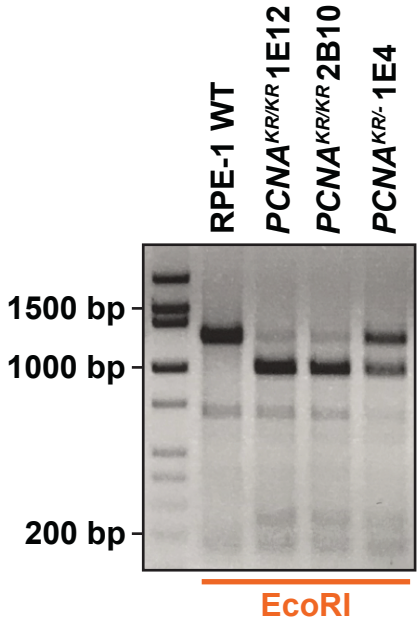

D.

Cell Line	Karyotype
RPE-1 WT	47, X, add(X)(q22), +12
PCNA$^{KR/KR}$ 1E12	94, X, add(X)(q22)(X)(q22), +12 +12
PCNA$^{KR/KR}$ 2B10	47, X, add(X)(q22), +12
PCNA$^{KR/-}$ 1E4	94, X, add(X)(q22)(X)(q22), del(X)(q13) +12 +12

E.

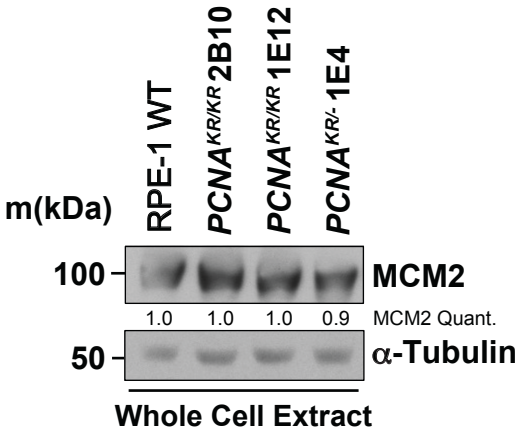

Figure S2. 293T *PCNA*^{K164R} mutant cells exhibit significant DNA synthesis defects

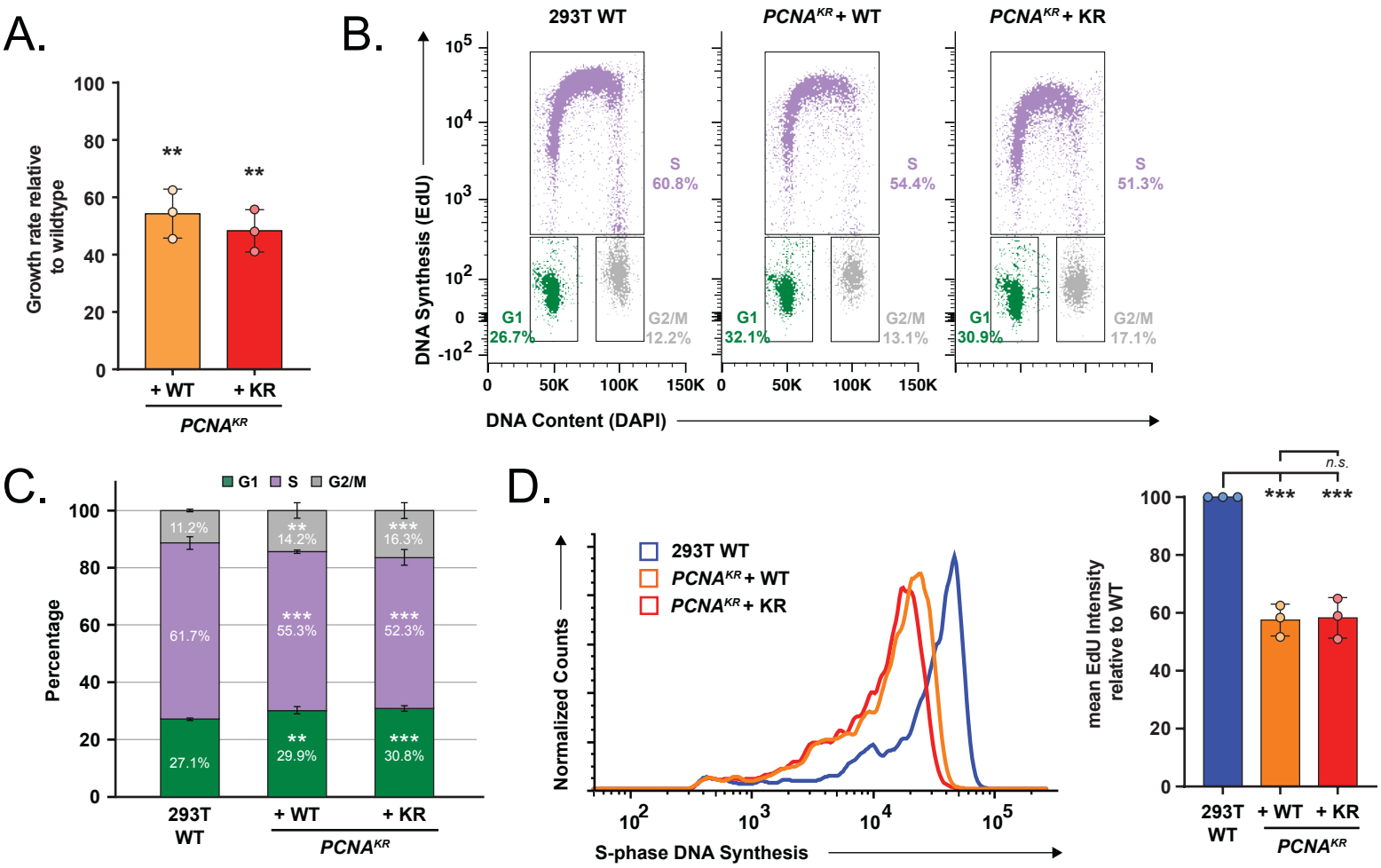

Figure S3. Reduced MCM2 loading in 293T *PCNA*^{K164R} cells

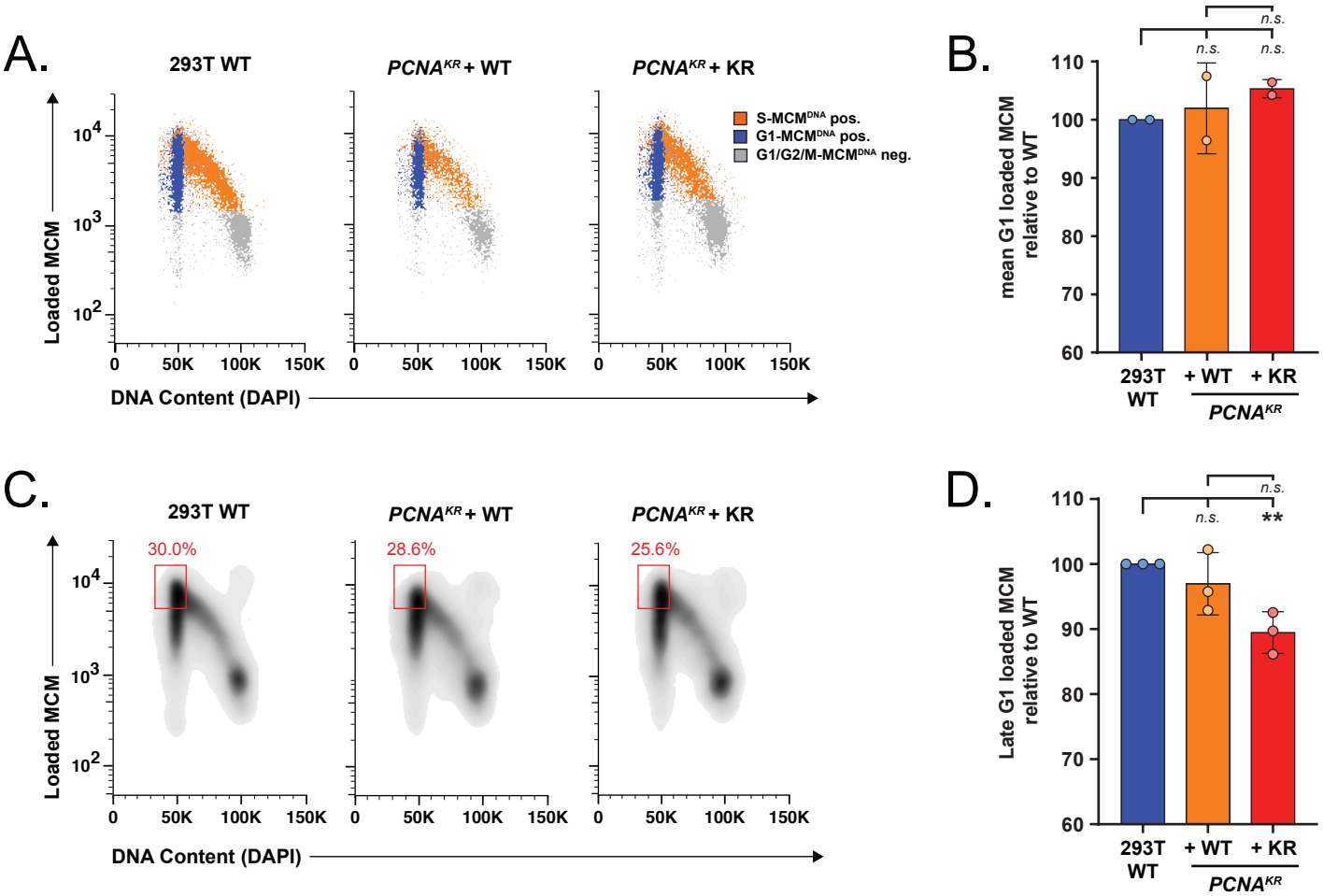

Figure S4. Replication defects in 293T *PCNA*^{K164R} cells

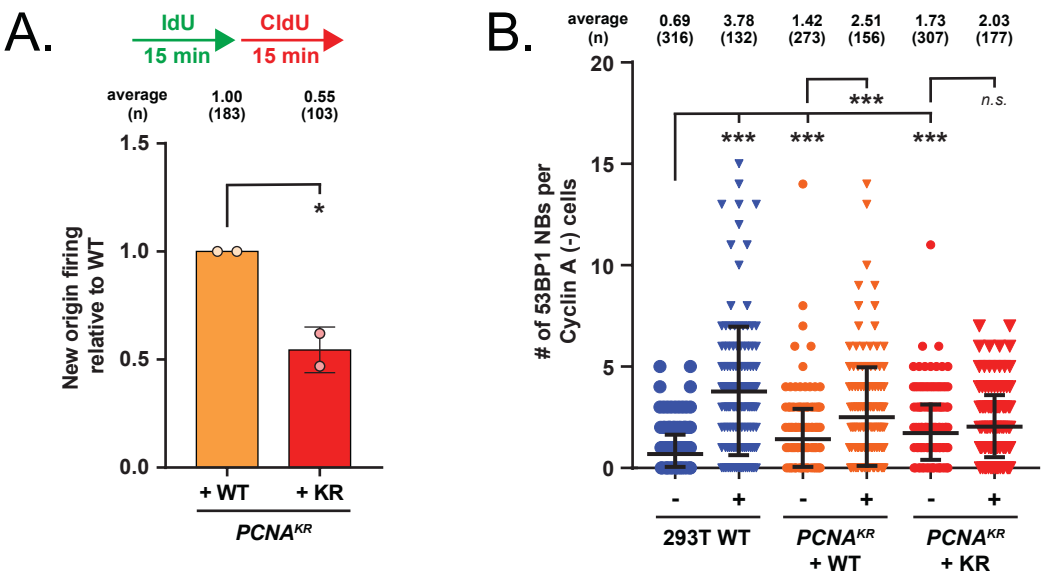

Figure S5. Enhanced MiDAS activation in MCM4 knockdown cells

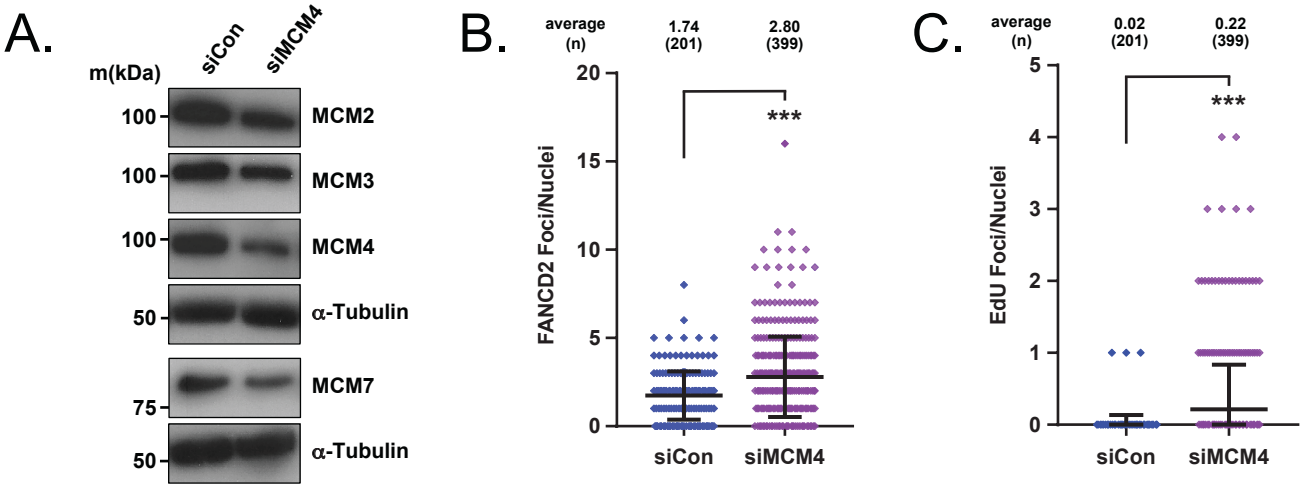
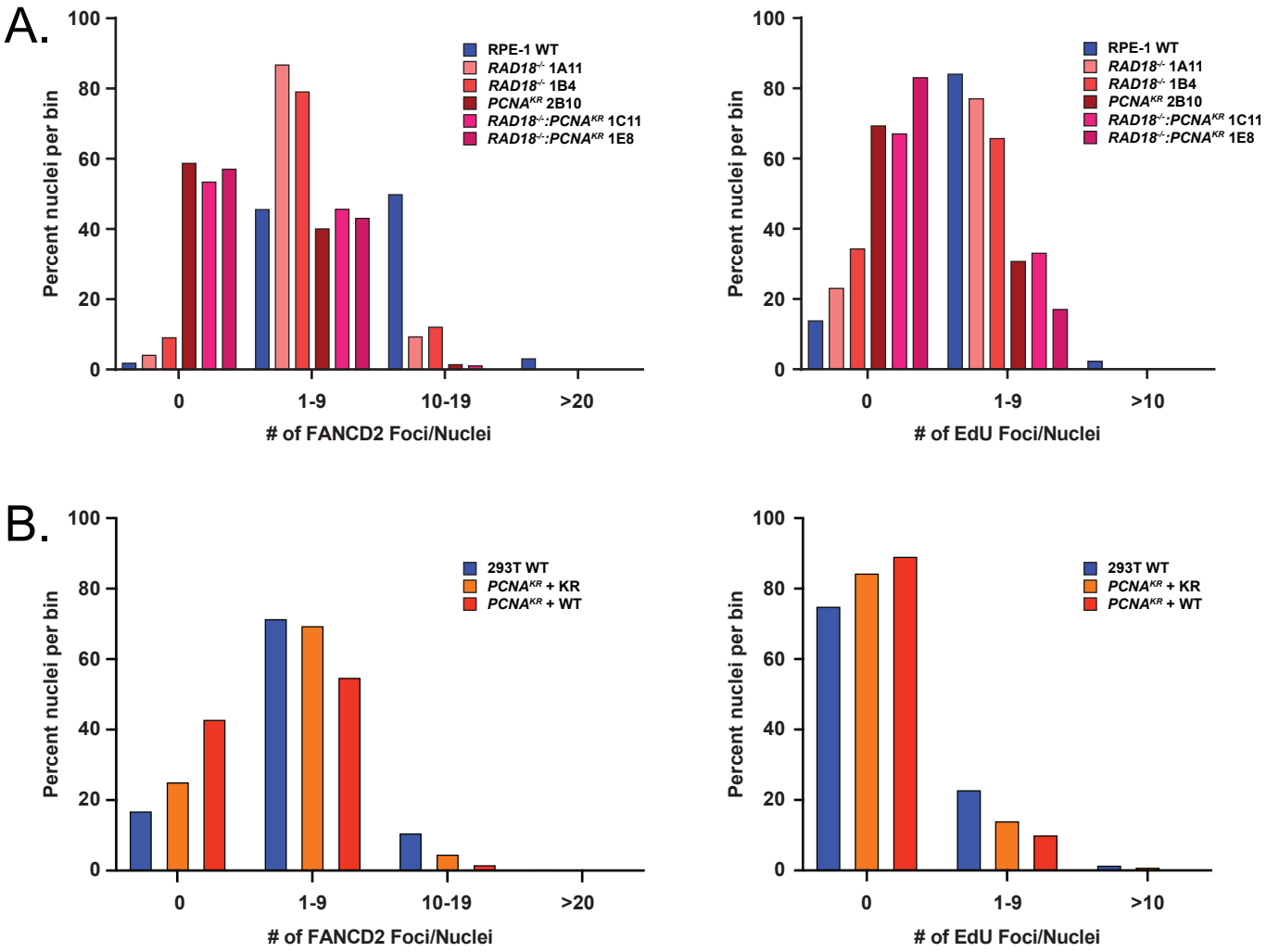
Figure S6. Reduced FANCD2 and EdU foci in *PCNA*^{K164R} mutants